Performance Analysis for Control- and User-Plane Separation based RAN with Non-Uniformly Distributed Users

Shuai Wang, Liqiang Zhao, *Member, IEEE*, Kai Liang, Gan Zheng, *Fellow, IEEE*, and Kai-Kit Wong, *Fellow, IEEE*

***Abstract*—In the control- and user-plane separation (CUPS) based radio access networks (RANs), control-signaling and data are transmitted by the control base stations (CBSs) and data base stations (DBSs), respectively. However, existing studies usually model the C/U-planes as two separate homogeneous networks, neglecting the dependence among the two planes and users. To address this problem, we analyze the coverage probability, spectrum efficiency (SE) and delay considering the dependent features among CBSs, DBSs, and non-uniformly distributed users based on stochastic geometry. Firstly, we present an analytical model for CUPS, where the DBSs are deployed at user hotspots based on Poisson point processes (PPPs), users are clustered around DBSs based on Poisson cluster processes (PCPs), and CBSs are deployed according to a dependent thinning of locations of DBSs based on Matérn hard-core processes (MHCPs). Secondly, we design novel distance-based fractional frequency reuse (FFR) schemes by exploiting the properties of PCP and MHCP to improve the coverage of cell edge users. Thirdly, we derive the distributions of user downlink rates, which are used to analyze the average queueing delay under M/M/C queueing model. Numerical results are presented to verify the efficiency of the proposed model compared to independently distributed BSs and users, and show the dependent BS deployment could significantly improve the coverage of the network.**

***Index Terms*—Cellular RANs, control- and user-plane separation, queueing theory, stochastic geometry, Poisson cluster process, Matérn hard-core processes, non-uniformly distributed users.**

This work was supported in part by the National Key R&D Program of China (2020YFB1807700), in part by Key-Area Research and Development Program of Guangdong Province (2020B0101120003), in part by the Key Research and Development Program of Shaanxi (2022KWZ-09), in part by the Postdoctoral Research Program of Shaanxi Province (2023BSHYDZZ100), in part by the National Postdoctoral Researcher Program (GZC20232058), and in part by the 111 Project (B08038). The work of Gan Zheng was supported in part by the National Natural Science Foundation of China (62071352), in part by the Royal Society International Exchanges grant (IEC\NSFC\181395).

Shuai Wang is with the State Key Laboratory of Integrated Services Networks, Xidian University, Xi'an 710071, China. (e-mail: wangshuaixidian@yeah.net).

Liqiang Zhao is with the State Key Laboratory of Integrated Services Networks, Xidian University, Xi'an 710071, China, and Guangzhou Institute of Technology, Xidian University, Guangzhou 510100, China. (e-mail: lqzhao@mail.edu.xidian.cn).

Kai Liang is with the School of Telecommunications Engineering, Xidian University, Xi'an 710071, China. (e-mail: kliang@xidian.edu.cn).

Gan Zheng is with the School of Engineering, University of Warwick, Coventry, CV4 7AL, UK (Email: gan.zheng@warwick.ac.uk).

Kai-Kit Wong is with the Department of Electronic and Electrical Engineering, University College London, London WC1E 6BT, U.K. (e-mail: kai-kit.wong@ucl.ac.uk).

I. Introduction

ALONG with the maturity of 5G mobile networks and the emerging 6G discussion [1], the future networks are expected to provide superior performance to support new service and applications. Meanwhile, the higher performance requirements and the scarcity of spectrum resources drive the exploitation of high-frequency bands, which also lead to shrinked coverage area due to the more complex channel environment and higher path loss [2]. On the other hand, one of the 6G visions is to provide full-dimensional wireless coverage [3], [4]. As a potential architecture for the wireless networks' coverage enhancement [5], control- and user-plane separation (CUPS) has been introduced in cellular radio access networks (RANs) as an emerging technology in mobile networks.

CUPS is the key feature of software defined networks (SDN) [6]. Inspired by SDN, the key concept of CUPS in RAN is to separate the signaling required for ubiquitous coverage from those needed to support high-speed data transmission [7]. In fact, the quantity of control signals is quite small compared with that of service data. On the other hand, high-speed data transmission and its related signaling have distinct characteristics and network requirements. Control signaling requires wide coverage and stable transmission, while data transmission focuses more on higher rates. This leads to a layered RAN architecture with a separation between the functionalities of network access and data transfer. The concept of CUPS will drive the mobile network towards the characteristics of flexibility and re-configurability with low cost.

Recently, many works have researched CUPS based cellular networks. To split the control-plane (C-plane) and user-plane (U-plane) in RANs, the control base stations (CBSs) and data base stations (DBSs) have been initially deployed in the same frequency band [8], in which the spectrum allocation to C/U-planes is optimized to achieve better spectrum efficiency (SE) and energy efficiency (EE). To provide ubiquitous coverage to cellular user, the collaborative high and low-frequency base station (BS) deployment relying on CUPS is put forward in [9], [10]. In [9], this architecture is introduced as phantom cellular networks, where a cell covered by a DBS is termed a phantom cell. Phantom cells are only in charge of data transmission in U-plane and operating on high-frequency bands. Meanwhile, their control signaling is carried by their supervising macro cells in C-plane, utilizing different frequency bands. The power and spectrum allocation of phantom cells has been

studied in [10] to optimize the EE and SE with imperfect channel state information (CSI). The utilization of a high-frequency band and shorter transmission distances in the U-plane introduces a more complex wireless environment, leading to the coexistence of line-of-sight (LoS) and non-line-of-sight (NLoS) transmissions. In this scenario, the SE, EE, and coverage have been analyzed in [11]. Additionally, the use of unlicensed bands in the U-plane has been explored in [12], [13]. Apart from the C/U-planes operating in LTE and mmWave bands, respectively, an assisting C-plane was deployed in the Wi-Fi band as an intermediate layer, forming a three-tier CUPS model in [14]. In [15], a cloud-based CUPS architecture was presented, where both CBSs and DBSs serve as remote radio heads (RRHs) and are connected to the virtual BS cloud through the fronthaul network. Further, benefiting from the flexible framework of CUPS, the storage units and computing units could be deployed on DBSs, to realize edge caching [16] and edge computing [17].

Several existing works use the homogeneous Poisson point process (PPP) to analyze network performance [18], [19], neglecting the non-uniform user distribution. While the PPP model has demonstrated accuracy in macro BS deployments in [20] through comparison with real-world data, it may not be entirely precise for certain dense urban HetNet cases when applied to the distribution of users and small BSs [21], [22]. As for the location of users, a common assumption is that users are distributed uniformly and are independent with BSs' locations. However, in reality, users' distribution is not always even and there exists hotspots where user gathering like shopping malls or airports. Fortunately, Poisson cluster process (PCP) is appropriate for modeling the non-uniformly distributed users [23], [24]. In addition, the non-independent deployment of small cells has also been considered in the 3GPP models for HetNets [25] , in which small BSs (SBSs) are deployed according to the user hotspots and users are clustered around SBSs. The spatial correlation of user and SBSs locations has been analyzed in [26], [27] and extended to many scenarios of interest in the literature like multi-tier HetNets in [28], [29] , device-to-device (D2D) networks in [30] , non-orthogonal multiple access (NOMA) networks in [31], [32] and uplink-downlink decoupling in [33]. Another shortcoming of PPP based network model is that it neglects the repulsive characteristics among BSs. Therefore, repulsive point processes including Poisson hard-core point process and Matérn hard-core processes (MHCPs) [34]–[40] are widely applied to capture the spatial repulsion in wireless networks.

In addition to the spatial distribution and channel conditions, traffic queuing at BSs also significantly impacts network performance [41]. Random service requests from users are aggregated at their associated BSs, and channels are allocated for data transfer. Queueing models have been applied to analyze the traffic conditions according to different network models, including $M/M/1$ [42], $M/M/C/C$ [11], $M/G/1$ [43] and interacting queues [41], [44]. [45]–[47] adopt the mean-field approximation to settle the "interacting queue" problem. However, in the case of a non-uniform and non-homogeneous spatial network model, introducing this method would amplify the challenges of analysis. Another assumption proposed by [11], [48], [49] posits that the channel allocation time or channel holding time follows an exponential distribution, simplifying performance analysis.

To manage the interference in the HetNet and improve the edge coverage, several frequency reuse (FR) techniques have been investigated, including fractional frequency reuse (FFR), soft FFR, FFR3, etc. [50]. The basic idea of FFR is to partition the cell into interior and edge regions and assign with different sub-bands. In conventional grid-based cellular network, the region partition is based on a predetermined distance, which is not applicable of stochastic geometry modeled network as the cells has irregular sizes and shapes [51]. To address this problem, [52], [53] categorize the interior and edge users based on SINR threshold. However, the time-varying instantaneous SINR may lead to random switching between interior and edge users. In [51], [54], a distance-based FFR is introduced to the network based on PPP, where the user classification is according to their distance from their associated and dominant interfering BS. However, the distance-based FFR has not been well investigated in network based on other stochastic geometry model based network like PCP and MHCP.

In this paper, we analyze the coverage probability, delay, and SE performance of RAN relying on CUPS based on PCPs and MHCPs. To the best of our knowledge, the dependent features among CBSs, DBSs and non-uniformly distributed users have not been investigated in the existing research on CUPS. The contributions of this paper are summarized as follows.

1) A hybrid MHCP-PCP network model: Existing research neglects the interdependency among CBSs, DBSs, and users. Therefore, we propose a hybrid network model for CUPS that accommodates these interdependent features through a comprehensive use of PCPs and MHCPs. This model aligns with the characteristics of CUPS, where capacity-driven DBSs are placed closer to users, while CBSs providing wider coverage are more sparse and repulsive. Specifically, DBSs are deployed at user hotspots based on PPPs, users are clustered around DBSs based on PCPs, and CBSs are deployed according to a dependent thinning of locations of DBSs based on MHCPs.

2) Distance-based fractional frequency reuse: In order to enhance overall coverage performance and mitigate inter-cell interference for cell-edge users, we propose two novel distance-based FFR techniques for control plane and user plane, respectively. Instead of the conventional SINR threshold-based classification, which often leads to random switching, the proposed distance-based classification in the U-plane is achieved by comparing the user's distance with the center DBS and the nearest non-center DBS. In the C-plane, the proposed method is realized by utilizing the hard-core distance.

3) Performance analysis based on M/M/C queueing model and stochastic geometry: The CBSs, DBS, and users are dependent in the proposed model. Meanwhile, the proposed FFR techniques separately analyze the interior and edge user, which makes the analysis more complex and challenging. To this end, we derive analytical solutions of coverage probability and spectrum efficiency for both interior/edge users in C/U-planes, respectively. In addition, the distribution of downlink rate is derived to analyze the average queueing delay under

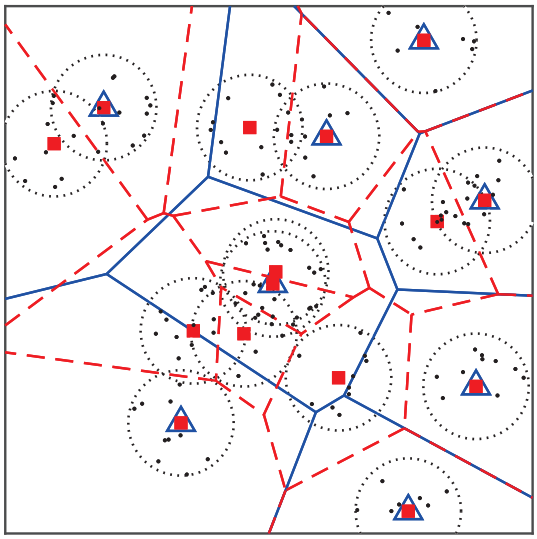

Fig. 1. The deployment of CBSs (blue triangles) following MHCPs, and DBSs (red squares) following HPPPs and the distribution of users (black dots) following PCPs.

$M/M/C$ queueing model, on covering the effects of inter-cell interference on delay.

The remainder of this paper are organized as follows. Section II introduces the system model of the proposed RAN relying on CUPS. Section III illustrates and analyzes the distance-based FFR model. Performance analyses of the U-plane and C-plane are presented in Section IV and Section V, respectively. Section VI provides the derivations of queueing delay. Numerical results and conclusions are presented in Section VII and Section VIII, respectively.

II. System Model

Consider a cellular network consisting of two kinds of BSs, named CBSs and DBSs, respectively. To be specific, the CBSs would take charge of transmitting signals in the C-plane, including control signaling; accordingly, the high-speed data would be transmitted through DBSs in the U-plane. The two kinds of BSs are assumed to work in different frequency bands, which means C-plane could take advantage of low frequency to guarantee the coverage of a wider area, while U-plane could benefits from the wide band in high frequency to achieve higher rate.

As illustrated in Fig. 1, we assume that all BSs and users are randomly deployed according to stochastic geometry. Specifically, the locations of DBSs follow independent homogeneous PPPs (HPPPs) Φ_d with a density of λ_d, CBSs are deployed based on MHCPs of Type II Φ_c, and user distribution follows PCPs.

Many existing studies modeled users as HPPPs independent with BSs. However, in practice, the location of users is spatially non-uniform [27]. To address this problem, many researches have focused on the user-centric capacity-driven small cell deployments [27], [28]. In [27], the locations of users and base stations are modeled as clustered around geographical centers of user hotspots. In [28], BSs are deployed at the center of user clusters to capture the location correlation between BSs and users. Since DBSs are responsible for high-speed data transmission, similar to [28], we assume that the deployment of DBSs is correlated with users' locations. This is analogous to small cells in regular HetNets that are deployed in crowded places such as malls and stations. On the other hand, users also prefer venues with stable and fast network service. Therefore, users tends to cluster around the DBSs once deployed. As a result, users are assumed to have clustered distributions following PCP [26].

A PCP consists of a parent PPP, and the clusters are scattered independently and with an identical spatial distribution around the points in the parent PPP. The user distribution is denoted by Φ_u, which follows a PCP with a cluster size S, representing the average number of users per cluster. Here, we assume that the parent process of Φ_u is equivalent to Φ_d so that DBSs are deployed at the cluster center of users. Any user's location follows an identical distribution with respect to the cluster center.

Here, the analysis is based on a commonly used PCP model: the Matérn cluster process (MCP). In the MCP, each user is uniformly distributed in a ball of radius R around the DBS, as shown by the dashed circle in Fig. 1. Therefore, the probability density function (PDF) of the users' locations relative to the DBSs in the MCP, denoted by $f_{\mathbf{X}}^{M}(\mathbf{x})$, is given by [56]

$$f_{\mathbf{X}}^{M}(\mathbf{x}) = \begin{cases} \frac{1}{\pi R^2} & , \quad \|\mathbf{x}\| \leq R \\ 0 & , \quad \text{otherwise.} \end{cases}, \tag{1}$$

where $\mathbf{x} = (y_0, \theta)$ represents the coordinates in the polar coordinate system. Here, y_0 denotes the distance between the user and its center DBS, and θ denotes the angle from the center DBS.

Since CBSs play a crucial role in assisting DBSs to maintain ubiquitous coverage, it is essential to consider the interdependence between the two planes. The low-frequency CBSs, responsible for wider coverage, result in a sparse and repulsive distribution. Consequently, we assume that the locations of CBSs follow a MHCP of Type II, denoted as Φ_c. Specifically, Φ_c is a dependent thinning of Φ_d with a minimum distance R_m between any two CBSs.

Φ_c is generated by assigning each point in Φ_d a mark uniformly distributed on the interval $[0, 1]$, and subsequently removing all points that have a neighbor within a distance of R_m with a smaller mark. The probability that a given CBS is retained is provided in [34], and it is given by

$$\mathcal{P}_r = \frac{1 - \exp(-\pi\lambda_d R_m^2)}{\pi\lambda_d R_m^2}. \tag{2}$$

The density of Φ_c is accordingly $\lambda_c = \mathcal{P}_r\lambda_d$.

The BSs in both the C-plane and U-plane employ orthogonal frequency-division multiplexing (OFDM) to support multiple users. Additionally, CBSs and DBSs operate in different frequency bands, so that they do not interfere with each other.

The BSs will communicate with users in the downlink based on users' requests, and the Signal-to-Interference-plus-Noise Ratio (SINR) for a typical C-plane user and a typical U-plane

user is given by

$$SINR_c = \frac{P_c h_c A_c R_c^{-\nu_c}}{\sum_{k\in\Phi_c^I} P_c h_k A_c R_k^{-\nu_c} + n_c}, \tag{3}$$

and

$$SINR_d = \frac{P_d h_d A_d R_d^{-\nu_d}}{\sum_{k\in\Phi_d^I} P_d h_k A_d R_k^{-\nu_d} + n_d}, \tag{4}$$

where P_c and P_d denote the transmit power of CBSs and DBSs, respectively. h_c, h_d, h_k represent the channel gains from the associated CBS/DBS and the k-th interfering BS to the typical user, respectively. R_c, R_d, and R_k denote the distance from the associated CBS/DBS and the k-th interfering BS to the typical user, respectively. Additionally, we assume that all channel gains follow the exponential distribution with a parameter of 1. ν_c and ν_d denote the path loss exponent in C/U-planes, A_c and A_d denote the corresponding path gain at a reference distance of 1 meter in C/U-planes, and n_c and n_d denote the noise power in C/U-planes, respectively. Φ_c^I and Φ_d^I represent the sets of interfering neighboring CBSs/DBSs, respectively, whose density will be derived in the following sections. The subscripts c and d represent CBS and DBS in the C/U-planes, respectively.

III. Frequency Reuse Model

The cell-edge users suffer from severe inter-cell interference, as they receive weaker signal power but stronger interference than cell-center users (also known as interior users) from neighboring BSs. To mitigate the inter-cell interference of edge users, several frequency reuse techniques have been put forward, including FFR, soft FFR, etc. Here we apply FFR for our system, and the main idea is to allocate different sub-bands for edge and interior users.

One of the key concerns of FFR is the classification of edge and interior users. Initially, the distance-based classification is widely applied in grid-based network analysis [50]. However, this method is not suitable for the random and irregular cell shape in networks modeled by stochastic geometry. In [52], [53], the classification in a PPP network is based on SINR threshold, i.e., users with SINR greater than a predetermined value would be regarded as interior users. Otherwise, they would be regarded as edge users. A distance-based classification method is introduced in [51], [54] in which users would be seen as edge users if the ratio between their distance from the serving BS and the dominant interfering BS (i.e., the second nearest BS) is less than a predetermined threshold. Inspired by that, we propose two novel user classification methods for C/U-plane users, respectively, based on the properties of MHCPs and PCPs.

A. Distance-based FFR for U-plane

Since there exists a center DBS D_0 for each cluster of users, whose distances from users are bounded by a small cluster radius R, D_0 could become either the serving BS or one of the powerful interference sources. Similar to [51], [54] which classify edge and interior users according to their distance from their serving and dominant interfering BSs, for the U-plane, the classification is according to the distance between the user with the cluster center DBS D_0 and the nearest non-center DBS D_1, i.e., R_0 and R_1, which is shown as follows.

All the DBSs are divided into two tiers: one is Φ_{d0}, which only includes the cluster center DBS (denoted by D_0) of the typical user, and the other is $\Phi_{d1} = \Phi_d \backslash D_0$, which contains all DBSs except D_0. Φ_{d1} still follows HPPP with the same density as Φ_d according to the *Slivnyak Theorem* [56]. We denote the nearest DBS in Φ_{d1} as D_1.

Since there is overlapping between clusters, D_0 may not be the nearest DBS. Therefore, we term the user as U-plane cluster interior user (UIU) if $R_0 < R_1$, as it is closer to the cluster center rather than DBSs in other clusters; otherwise, it is termed as U-plane cluster edge user (UEU). Therefore, the probability that the typical user is classified as UIU is derived by comparing R_0 and R_1 as $\mathcal{P}_{d,i} = \mathbb{P}(R_0 < R_1)$, and the probability that a typical user is a UEU is $\mathcal{P}_{d,e} = 1 - \mathcal{P}_{d,i}$.

The distribution of R_0 is the marginal distribution of (1) by integrating over θ (i.e., the angle from the center DBS to the typical user) in polar coordinates. We denote the PDF and cumulative distribution function (CDF) of R_0 as $f_{R_0}(r_0)$ and $F_{R_0}(r_0)$, which are given by, respectively,

$$f_{R_0}(r_0) = \begin{cases} \frac{2r_0}{R^2} & , \quad 0 \le r_0 \le R \\ 0 & , \quad otherwise \end{cases}, \tag{5}$$

and

$$F_{R_0}(r_0) = \frac{r_0^2}{R^2}, \quad 0 \le r_0 \le R. \tag{6}$$

Note that although the typical user is dependent on D_0, the independence still holds between the typical user and the other DBSs except D_0. Since Φ_{d1} still follows the HPPP, if we denote the distance between the typical user and D_1 as R_1, the PDF and CDF of R_1 are

$$f_{R_1}(r_1) = 2\pi\lambda_d r_1 \exp(-\pi\lambda_d r_1^2), \tag{7}$$

and

$$F_{R_1}(r_1) = 1 - \exp(-\pi\lambda_d r_1^2). \tag{8}$$

Then $\mathcal{P}_{d,i}$ is given by

$$\mathbb{P}(R_0 < R_1) = \mathbb{E}_{R_0}[\overline{F}_{R_1}(R_0)] = \frac{1 - \exp(-\pi\lambda_d R^2)}{\pi\lambda_d R^2}. \tag{9}$$

and $\mathcal{P}_{d,e} = 1 - \mathcal{P}_{d,i}$.

When classified as a UIU, the distribution of R_0 changes accordingly to a conditional distribution. For instance, D_0 being the nearest DBS implies that R_0 is smaller than R_1. Therefore, the distribution of R_0 should be conditioned on $R_0 < R_1$. The conditional CDF of R_0, denoted as $F_{R_0}^{d,i}(t)$, is given by

$$\begin{aligned} & \mathbb{P}(R_0 < r_0 \mid R_0 < R_1) \\ = \; & \frac{\mathbb{P}(R_0 < r_0, R_0 < R_1)}{\mathbb{P}(R_0 < R_1)} \\ \overset{(a)}{=} \; & \frac{1}{\mathcal{P}_{d,i}} \int_0^t \left(\int_{r_0}^{\infty} f_{R_1}(r_1) \mathrm{d}r_1 \right) f_{R_0}(r_0) \mathrm{d}r_0 \\ = \; & \frac{1}{\mathcal{P}_{d,i}} \int_0^t \overline{F}_{R_1}(r_0) f_{R_0}(r_0) \mathrm{d}r_0, \end{aligned} \tag{10}$$

where (a) holds due to $\mathcal{P}_{d,i} = \mathbb{P}(R_0 < R_1)$, and the limits

$R_0 < t$ and $R_0 < R_1$ define the integral range. Consequently, $f_{R_0}^{d,i}(r_0)$ is the derivative of $F_{R_0}^{d,i}(r_0)$ with respect to r_0, and it is expressed as

$$f_{R_0}^{d,i}(r_0) = \frac{1}{\mathcal{P}_{d,i}} \overline{F}_{R_1}(r_0) f_{R_0}(r_0). \tag{11}$$

The conditional distribution of R_1 when the typical user is classified as a UEU will be obtained in the same way:

$$f_{R_1}^{d,e}(r_1) = \frac{1}{\mathcal{P}_{d,e}} \overline{F}_{R_0}(r_1) f_{R_1}(r_1). \tag{12}$$

Here, we set the reuse factor K_d. Therefore, all the DBSs would transmit to the UIU using a certain frequency band. The remaining frequency band is divided into K_d orthogonal sub-bands, and each DBS randomly selects one of the K_d sub-bands for the UEUs. So, for the UEU, the interfering probability is $\mathcal{P}_{d,e}^I = 1/K_d$, while for UIU $\mathcal{P}_{d,i}^I = 1$.

B. Distance-based FFR for C-plane

For the C-plane, we assume that the classification is determined by the hard-core distance R_m. In the proposed model based on MHCPs, the deployment of CBSs is a dependent thinning of Φ_d, and each two CBSs have a minimum distance R_m. If the distance between two nodes within Φ_d is less than R_m, only one node is retained as a CBS. Specifically, if the cluster center of the typical user is retained as CBS, the users are categorized as C-plane cell interior users (CIUs), otherwise as C-plane cell edge users (CEUs). As a result, the probability of a user being CIU is equal to the retaining probability of MHCP in (2) as $\mathcal{P}_{c,i} = \mathcal{P}_r$, while the probability of a user being CEU is $\mathcal{P}_{c,e} = 1 - \mathcal{P}_r$.

Accordingly, each CBS applies a dedicated band for CIU and randomly selects one of K_c sub-bands for CEUs. The interfering probabilities for CIUs and CEUs are $\mathcal{P}_{c,i}^I = 1$ and $\mathcal{P}_{c,e}^I = 1/K_c$, respectively.

IV. Performance Analysis of User Plane

In this part, we will analyze the performance of DBSs in the U-plane. We assume the Max Power Association (MPA) for user-BS association, which means that the typical user would choose the nearest DBS, i.e., the nearest one between D_0 and D_1. Note that, the performance analysis in this section are conducted conditioned on the users are under the coverage of CBSs.

The interfering neighboring DBSs denoted by Φ_d^I is a part of DBSs that reuse the same channel with the typical user. The density of Φ_d^I is $\lambda_d^I = \mathcal{P}_d^I \lambda_d$, due to that both Φ_{d1} and Φ_{d1}/D_1 follow HPPP and have densities of λ_d under *Slivnyak Theorem*.

We define $\mathcal{C}_d$ as the coverage probability in U-plane and it could be express by

$$\mathcal{C}_d = \mathbb{P}(SINR_d > \gamma_d), \tag{13}$$

where γ_d is the threshold.

A. Conditional Coverage Probability for UIUs

Based on the MPA, the user will connect to the DBS which could provide the maximum expected received power. In the U-plane, there exists two cases, which depend on whether the DBS at users' cluster center (i.e., D_0) or the nearest DBS in Φ' (i.e., D_1) could provide the typical user with the maximum received power. Note that, in the U-plane, the interior users and edge users are also categorized under the same criterion. In the two cases, some key values like the interference power and contact distances are calculated in different manners. Therefore, the coverage probability of UIU and UEU are derived respectively.

The UIUs are closer to D_0 and therefore associated with D_0, the PDF of contact distance is $f_{R_0}^{d,i}(r_0)$ in (11), and the interfering neighboring DBSs are no closer than D_0, so the coverage probability is given by

$$\begin{aligned}
&\mathbb{P}(SINR_d > \gamma_d) \\
= \;& \mathbb{P}\left(h_d > \frac{\gamma_d}{P_d A_d R_d^{-\nu_d}} \Big(\sum_{k \in \Phi_d^I} P_d A_d h_k R_k^{-\nu_d} + n_0 \Big) \right) \\
\overset{(b)}{=} \;& \mathbb{E}_{R_d}\left[\exp\left(-\mathcal{N}_d R_d^{\nu_d}\right) \exp\left(-\gamma_d R_d^{\nu_d} I_d\right) \right] \\
= \;& \int_0^R \exp\left(-\mathcal{N}_d r_0^{\nu_d}\right) \mathcal{L}_{I_d}\left(\gamma_d r_0^{\nu_d}\right) f_{R_0}^{d,i}(r_0) \mathrm{d}r_0, \\
= \;& \frac{1}{\mathcal{P}_{d,i}} \int_0^R \exp\left(-\mathcal{N}_d r_0^{\nu_d}\right) \\
& \cdot \mathcal{L}_{I_d}\left(\gamma_d r_0^{\nu_d}\right) \overline{F}_{R_1}(r_0) f_{R_0}(r_0) \mathrm{d}r_0,
\end{aligned} \tag{14}$$

where (b) holds because h_d following exponential distribution. Denote $s = \gamma_d r_0^{\nu_d}$, $\mathcal{L}_{I_d}(s)$ only contains interference component from Φ_{d1}, which is

$$\begin{aligned}
& \mathbb{E}\left[\exp\left(-s \sum_{k \in \Phi_{d1}} h_k r_k^{-\nu_d} \right) \right] \\
= \;& \mathbb{E}\left[\prod_{k \in \Phi_{d1}} \exp\left(-s h_k R_k^{-\nu_d}\right) \right] \\
\overset{(c)}{=} \;& \exp\left(-2\pi \lambda_d^I \int_{r_0}^{\infty} \left(1 - \mathbb{E}_h\left[\mathrm{e}^{-s h r^{-\nu_d}} \right]\right) r \mathrm{d}r \right) \\
\overset{(d)}{=} \;& \exp\left(-2\pi \lambda_d^I \int_{r_0}^{\infty} \left(1 - \frac{1}{1 + s r^{-\nu_d}} \right) r \mathrm{d}r \right) \\
= \;& \exp\Bigg(-2\pi \lambda_d \frac{s r_0^{2-\nu_d}}{\nu_d - 2} \cdot \\
& {}_2F_1\left[1, 1 - \frac{2}{\nu_d}, 2 - \frac{2}{\nu_d}, -r_0^{-\nu_d} s \right] \Bigg),
\end{aligned} \tag{15}$$

where ${}_2F_1[x, y, z, w]$ is a Gauss Hypergeometric function, (c) holds due to the probability generating functional (PGFL) of PPP [56] and no interfering DBS closer than r_0, (d) is because all h_k follow i.i.d exponential distributions.

Substituting (15) into (14), we could derive the conditional coverage probability for the UIUs as

$$\mathcal{C}_{d,i} = \frac{1}{\mathcal{P}_{d,i}} \int_0^R \exp\left(\mathcal{G}_d r_0^2 - \mathcal{N}_d r_0^{\nu_d} \right) \frac{2 r_0}{R^2} \mathrm{d}r_0, \tag{16}$$

where $\mathcal{G}_d = -\pi\lambda_d(\frac{2\gamma_{d\,2}F_1\left[1,1-\frac{2}{\nu_d},2-\frac{2}{\nu_d},-\gamma_d\right]}{\nu_d-2}+1)$ and $\mathcal{N}_d = \frac{\gamma_d n_0}{P_d A_d}$.

B. Conditional Coverage Probability for UEUs

In this part, we will derive the conditional probability $\mathcal{C}_{d,e}$ when the typical user is associated with D_1, which is the nearest DBS in Φ_{d1}. So there coexists interference from D_0 and Φ_{d1}/D_1, denoted by I_0 and I_1, respectively. Following the same procedure, we need to obtain the Laplace transform of I_0 and I_1, which are denoted by $\mathcal{L}_{I_0}$ and $\mathcal{L}_{I_1}$, respectively.

The derivation of $\mathcal{L}_{I_1}$ is similar to (15), except that in this case, the lower limit of the integral is r_1 and is given by

$$\begin{aligned}\mathcal{L}_{I_1}(s) &= \mathbb{E}\left[\exp\left(-s\sum_{k\in\Phi_d^I} h_k r_k^{-\nu_d}\right)\right]\\ &= \exp\left(-2\pi\lambda_d^I\int_{r_1}^{\infty}\mathbb{E}_h\left[1-\mathrm{e}^{-shr^{-\nu_d}}\right]r\mathrm{d}r\right)\\ &= \exp\left(-2\pi\frac{\lambda_d}{K_d}\frac{s r_1^{2-\nu_d}}{\nu_d-2}\cdot\right.\\ &\quad \left.{}_2F_1\left[1,1-\frac{2}{\nu_d},2-\frac{2}{\nu_d},-r_1^{-\nu_d}s\right]\right),\end{aligned} \tag{17}$$

Substitute $s=\gamma_d r_1^{\nu_d}$ into (17), we derive that

$$\mathcal{L}_{I_1}(\gamma_d r_1^{\nu_d}) = \exp\left(\mathcal{G}_d' r_1^2\right), \tag{18}$$

where $\mathcal{G}_d' = -2\pi\frac{\lambda_d}{K_d}\frac{\gamma_{d\,2}F_1\left[1,1-\frac{2}{\nu_d},2-\frac{2}{\nu_d},-\gamma_d\right]}{\nu_d-2}$.

$\mathcal{L}_{I_0}$ is more difficult to derive due to the spatial relationship between D_0 and the typical user. Similar to other DBSs, D_0 also has a probability of $1/K_d$ to generate interference on the typical users. As a result, $\mathcal{L}_{I_0}$ can be calculated by

$$\begin{aligned}&\mathbb{E}_{I_0}\left[\exp\left(-sI_0\right)\right]\\ \overset{(e)}{=}\ &\frac{1}{K_d}\mathbb{E}_{r_0,h_0}\left[\exp\left(-sh_0 r_0^{-\nu_d}\right)\right]+(1-\frac{1}{K_d})\exp(0)\\ \overset{(f)}{=}\ &\frac{1}{K_d}\mathbb{E}_{r_0}\left[\frac{1}{1+sr_0^{-\nu_d}}\right]+1-\frac{1}{K_d},\end{aligned} \tag{19}$$

where h_0, r_0 are the channel gain and distance between D_0 and user, (e) holds because when D_0 is not an interference source, $I_0=0$ and thus $\exp(-sI_0)=1$ with a probability $1-1/K_d$, (f) holds because h_0 follows exponential distribution.

The PDF of r_0 is derived from (5). However, since D_0 is not the nearest DBS, the calculation of the PDF needs to account for the location of D_1. When $R_1=r_1$, the PDF of R_0 becomes $f_{R_0}(r_0 \mid r_0>r_1) = \frac{f_{R_0}(r_0)}{\overline{F}_{R_0}(r_1)}$. Then, $\mathcal{L}_{I_0}$ is derived as

$$\begin{aligned}&\frac{1}{K_d}\mathbb{E}_{r_0}\left[\frac{1}{1+sr_0^{-\nu_d}}\right]+1-\frac{1}{K_d}\\ =\ &\frac{1}{K_d}\int_{r_1}\frac{1}{1+sr_0^{-\nu_d}}\frac{f_{r_0}(r_0)}{\overline{F}_{r_0}(r_1)}\mathrm{d}r_0+1-\frac{1}{K_d}\\ =\ &\frac{1}{K_d}\int_{r_1}^{R}\frac{1}{1+sr_0^{-\nu_d}}\frac{2r_0}{R^2-r_1^2}\mathrm{d}r_0+1-\frac{1}{K_d}\\ =\ &1-\frac{1}{K_d}\frac{R^2\mathcal{G}_1-r_1^2\mathcal{G}_2}{R^2-r_1^2},\end{aligned} \tag{20}$$

which has the closed-form solution, where $\mathcal{G}_1 = {}_2F_1[1,\frac{2}{\nu_d},1+\frac{2}{\nu_d},-\frac{R^{\nu_d}}{\gamma_d r_1^{\nu_d}}]$ and $\mathcal{G}_2 = {}_2F_1[1,\frac{2}{\nu_d},1+\frac{2}{\nu_d},-\frac{1}{\gamma_d}]$.

Considering the coexistence of $\mathcal{L}_{I_0}$ and $\mathcal{L}_{I_1}$, $\mathcal{C}_{d,e}$ could be expressed as

$$\begin{aligned}\mathbb{P}(SINR_d>\gamma_d) = &\int_0^R \exp\left(-\mathcal{N}_d r_1^{\nu_d}\right)\\ &\cdot\mathcal{L}_{I_0}\left(\gamma_d r_1^{\nu_d}\right)\mathcal{L}_{I_1}\left(\gamma_d r_1^{\nu_d}\right)f_{R_1}^{d,e}(r_1)\mathrm{d}r_1.\end{aligned} \tag{21}$$

Substitute $\mathcal{L}_{I_0}$, $\mathcal{L}_{I_1}$ and $f_{R_1}^{d,e}(r_1)$ into (21), we could derive

$$\begin{aligned}\mathcal{C}_{d,e} = &\frac{1}{\mathcal{P}_{d,e}}\int_0^R \exp\left((\mathcal{G}_d'-\pi\lambda_d)r_1^2-\mathcal{N}_d r_1^{\nu_d}\right)\\ &\cdot\left(1-\frac{1}{K_d}\frac{R^2\mathcal{G}_1-r_1^2\mathcal{G}_2}{R^2-r_1^2}\right)2\pi\lambda_d r_1\left(1-\frac{r_1^2}{R^2}\right)\mathrm{d}r_1.\end{aligned} \tag{22}$$

Conditioned on the user being covered by a CBS, the overall coverage probability for users in the U-plane is given by

$$\mathcal{C}_d = \mathcal{P}_{d,i}\mathcal{C}_{d,i} + \mathcal{P}_{d,e}\mathcal{C}_{d,e}. \tag{23}$$

C. SE of U-Plane

The U-plane is responsible for high-speed data transmission, making Spectral Efficiency (SE) a crucial performance metric for U-plane users. Then we would provide the relationship between coverage probability and SE, which is denoted by η^{SE}.

Following a similar method to [20] and considering that $\mathbb{E}[X] = \int_{t>0}\mathbb{P}(X>t)\mathrm{d}t$ holds for any positive random variable X, we can derive η as follows:

$$\begin{aligned}\eta^{SE} &= \mathbb{E}[\log_2(1+SINR)]\\ &= \frac{1}{\ln 2}\int_0^{\infty}\mathbb{P}[\ln(1+SINR)>t]dt\\ &= \frac{1}{\ln 2}\int_0^{\infty}\mathbb{P}[SINR>\mathrm{e}^t-1]dt\\ &= \frac{1}{\ln 2}\int_0^{\infty}\mathcal{C}(\mathrm{e}^t-1)dt.\end{aligned} \tag{24}$$

By substituting $\gamma=\mathrm{e}^t-1$ into (24), where $t=\ln(1+\gamma)$ and $\mathrm{d}t = 1/(1+\gamma)\mathrm{d}\gamma$, and adjusting the integral range accordingly, the SE can be obtained. Hence, with the given coverage probability, the ergodic SE of the typical user is given by

$$\eta_d^{SE} = \frac{1}{\ln 2}\int_0^{\infty}\frac{\mathcal{C}_d(\gamma)}{1+\gamma}\mathrm{d}\gamma. \tag{25}$$

V. Performance Analysis of Control Plane

Since the control signaling in C-plane is required for the U-plane transmission, the coverage probability of the C-plane has an effect on the overall system performance. With the distance-based FFR schemes introduced in Section III-B, the coverage probability of the C-plane could be derived using properties of MHCPs and PCPs.

The coverage probability of the C-plane is defined as the probability that the SINR is greater than a threshold, which is given by

$$\mathcal{C}_c = \mathbb{P}(SINR_c>\gamma_c), \tag{26}$$

where γ_c is the SINR threshold.

The location of CBSs Φ_c follows MHCPs, which is a dependent thinning of Φ_d. To take advantage of the better coverage of CBSs, we assume that $R_m \geq 2R$. In other words, the minimum distance between each pair of CBSs is no smaller than twice the cluster radius to avoid the overlapping of coverage areas for each CBS.

In the C-plane, users follow MPA, which means users will connect to their nearest CBSs because they could provide the maximum expected received power. The coverage analysis of C-plane depends on whether the cluster center of the typical user is retained as CBS.

A. Coverage probability for CIU

The CIUs are the users whose cluster centers are retained as CBSs, which are denoted by C_0. Therefore, C_0 shares the location with the center DBS D_0. Since $R_m \geq 2R$, the nearest CBS of the typical user is C_0. Thus, the distance between the typical user and C_0, denoted by R_{C_0}, is same with R_0, and the PDF of R_{C_0} is given by

$$f_{R_{c_0}}^{c,i}(r_{c_0}) = \begin{cases} \frac{2r_{c_0}}{R^2} & , \quad 0 \leq r_{c_0} \leq R \\ 0 & , \quad otherwise \end{cases}, \tag{27}$$

Since the PGFL of the MHCP has not been found yet, the Laplace transform of the aggregate interference from interfering CBSs cannot be calculated exactly. To analyze the coverage of a network deployed following the MHCP, a conventional method is to approximate the MHCP by an equal-density PPP with a corresponding exclusion zone. The efficiency of the approximation is demonstrated in [34] and has been widely applied in the literature.

Therefore, in the case where C_0 is retained, $\mathcal{C}_{c,i}$ could be calculated as

$$\begin{aligned} & \mathbb{P}(SINR_c > \gamma_c) \\ = \; & \mathbb{P}\left(h_c > \frac{\gamma_c}{P_c A_c R_c^{-\nu_c}} \left(\sum_{k \in \Phi_c^I} P_c A_c h_k R_k^{-\nu_c} + n_0 \right) \right) \\ = \; & \int_0^R \exp\left(-\mathcal{N}_c r_{c0}^{\nu_c}\right) \mathcal{L}_{I_{c_0}}\left(\gamma_c r_{c0}^{\nu_c}\right) f_{R_{c_0}}^{c,i}(r_{c_0}) \mathrm{d}r_{c_0}, \end{aligned} \tag{28}$$

where $\mathcal{N}_c = \frac{\gamma_c n_0}{P_c A_c}$, $I_c = \sum_{k \in \Phi_c^I} h_k R_k^{-\nu_c}$, $\mathcal{L}_{I_{c_0}}(m)$ is the Laplace transform of I_c.

Denote $m = \gamma_c r_{c0}^{\nu_c}$, $\mathcal{L}_{I_{c_0}}(m)$ only contains the interference component from Φ_C / C_0, which is

$$\mathcal{L}_{I_{c_0}}(m) = \mathbb{E}\left[\exp\left(-m \sum_{k \in \Phi_c^I} h_k R_k^{-\nu_c} \right) \right], \tag{29}$$

where R_k is the distance between the typical user and the k-th interfering neighboring CBS.

Following the method in [35], the coordinate system is translated with setting C_0 at the origin and the typical user at the negative side of the x-axis, as shown in Fig. 2. Therefore, R_k is derived using the cosine rule, given by

$$R_k = \sqrt{(R_{c_0}^2 + r_i^2 + 2 r_i R_{c_0} \cos\phi)}, \tag{30}$$

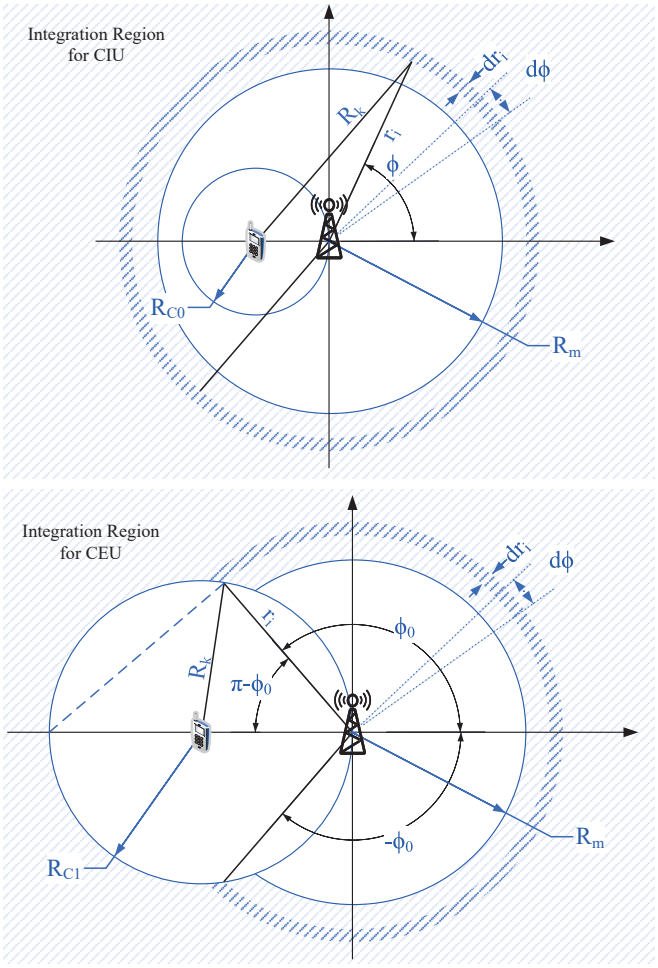

Fig. 2. Integration region for $\mathcal{L}_{I_{c_0}}(m)$ and $\mathcal{L}_{I_{c_1}}(m)$.

where $r_i = \|C_k - C_0\|$ represents the distance between the interfering CBS C_k and the associated CBS C_0.

As we assumed $R_m \geq 2R$, the integration region is illustrated in Fig. 2. Here we apply the PPP approximation and use the PGFL of PPP to calculate $\mathcal{L}_{I_{c_0}}(m)$, which is given by

$$\begin{aligned} & \mathbb{E}\left[\exp\left(-m \sum_{k \in \Phi_c^I} h_k R_k^{-\nu_c} \right) \right] \\ \approx \; & \exp\left(-\int_{R_m}^{\infty} \int_{-\pi}^{\pi} \mathbb{E}_h\left[1 - \mathrm{e}^{-mhR_k^{-\nu_c}} \right] \Lambda(r_i \mathrm{d}\phi \mathrm{d}r_i) \right) \\ = \; & \exp\left(-\int_{R_m}^{\infty} \int_{-\pi}^{\pi} \lambda_d \frac{k(r_i)}{\mathcal{P}_r} r_i \right. \\ & \left. \cdot \left(1 - \frac{1}{1 + m(r_{c_1}^2 + r_i^2 + 2 r_i r_{c_1} \cos\phi)^{\frac{-\nu_c}{2}}} \right) \mathrm{d}\phi \mathrm{d}r_i \right). \end{aligned} \tag{31}$$

where $\Lambda(r_i \, \mathrm{d}\phi \, \mathrm{d}r_i) = \frac{\lambda_d k(r_i)}{\mathcal{P}_r} \, \mathrm{d}\phi \, \mathrm{d}r_i$ is the conditional intensity of the approximated PPP [35], $k(r_i)$ is the probability of two points in the parent PPP separated by a distance r_i to be both retained in the resulting MHCP process, which is given

in [34] by

$$k(r_i)=\begin{cases} 0 & , \quad r<R_m \\ \frac{2\left(\frac{1-\mathrm{e}^{-\pi R_m^2\lambda_d}}{\pi R_m^2}+\frac{\mathrm{e}^{-\lambda_d V}-1}{V}\right)}{\lambda_d{}^2(V-\pi R_m^2)} & , \quad r\geq R_m \end{cases}, \tag{32}$$

where

$$V=\begin{cases} 2\pi R_m^2+\sqrt{R_m^2-\frac{r_i^2}{4}}r_i & , \quad r\leq 2R_m \\ -2\arccos(\frac{r_i}{2R_m})R_m^2 & \\ 2\pi R_m^2 & , \quad r>2R_m \end{cases}. \tag{33}$$

Substitute (31) into (28), we have

$$\mathcal{C}_{c,i}=\int_0^R \exp\left(-\mathcal{N}_c r_{c_0}^{\nu_c}\right)\mathcal{L}_{I_{c_0}}\left(\gamma_c r_{c_0}^{\nu_c}\right)\frac{2r_{c_0}}{R^2}\mathrm{d}r_{c_0}, \tag{34}$$

where $\mathcal{N}_c=\frac{\gamma_c n_0}{P_c A_c}$ and $\mathcal{L}_{I_{c_0}}\left(\gamma_c r_{c_0}^{\nu_c}\right)$ is given by

$$\mathcal{L}_{I_{c_0}}\left(\gamma_c r_{c_0}^{\nu_c}\right)=\exp\left(-\int_{R_m}^{\infty}\int_{-\pi}^{\pi}\lambda_d\frac{k(r_i)}{\mathcal{P}_r}r_i \cdot\left(1-\frac{1}{1+\gamma_c r_{c_0}^{\nu_c}(r_{c_0}^2+r_i^2+2r_i r_{c_0}\cos\phi)^{\frac{-\nu_c}{2}}}\right)\mathrm{d}\phi\mathrm{d}r_i\right). \tag{35}$$

B. Coverage probability for CEU

In contrast, if the cluster center is not retained as a CBS, the typical user is categorized as a CEU and associated with the nearest CBS, which is denoted by C_1. Note that the residual points Φ_d/Φ_c form another process named the complementary-MHCP (CMHCP). However, it has been proved through simulation [36], [37] that the correlation between the CMHCP and the MHCP thinning from the same parent process is insignificant, and the CMHCP can be approximated as an independent PPP.

Although there is no known closed-form expression for the contact distance based on MHCP, we adopt an approximated distribution, which has been proven to be sufficiently accurate and has been widely applied in the literature [38]–[40], conditioned on the maximum distance between CEU and its associated CBS being R_m+R. The PDF of the contact distance between the typical user and its associated CBS is given by

$$f_{R_{c_1}}^{c,e}(r_{c_1})=\frac{2\pi\lambda_c r_{c_1}\exp(-\pi\lambda_c r_{c_1}^2)}{1-\exp(-\pi\lambda_c(R+R_m)^2)}. \tag{36}$$

In case C_0 is not retained, $\mathcal{C}_{c,e}$ is expressed as

$$\begin{aligned}&\mathbb{P}(SINR_c>\gamma_c)\\ =&\int_0^R \exp\left(-\mathcal{N}_c r_{c_0}^{\nu_c}\right)\mathcal{L}_{I_{c_1}}\left(\gamma_c r_{c_1}^{\nu_c}\right)f_{R_{c_1}}^{c,e}(r_{c_1})\mathrm{d}r_{c_1},\end{aligned} \tag{37}$$

where $\mathcal{L}_{I_{c_1}}(m)$ is the Laplace transform of aggregated interference from Φ_c/C_1.

The derivation of $\mathcal{L}_{I_{c_1}}(m)$ is similar to $\mathcal{L}_{I_{c_0}}(m)$. However, in this case, as the typical user is not in the cluster centered at C_1, there exists the situation that $r_i<2R_{c_1}$, which reshapes the integration region.

In this case, the upper and lower limits of the integral are changed accordingly, as shown in Fig. 2. Due to this, $\mathcal{L}_{I_{c_1}}(m)$ is given by

$$\begin{aligned}&\mathbb{E}\left[\exp\left(-m\sum_{k\in\Phi_c^I}h_k r_k^{-\nu_c}\right)\right]\\ \approx&\exp\left(-\int_{R_m}^{\infty}\int_{-\phi_0}^{\phi_0}\mathbb{E}_h\left[1-\mathrm{e}^{-mhr_k^{-\nu_c}}\right]\Lambda(r_i\mathrm{d}\phi\mathrm{d}r_i)\right)\\ =&\exp\left(-\int_{R_m}^{\infty}\int_{-\phi_0}^{\phi_0}\frac{\lambda_d}{K_c}\frac{k(r_i)}{\mathcal{P}_r}r_i \cdot\left(1-\frac{1}{1+m(r_{c_1}^2+r_i^2+2r_i r_{c_1}\cos\phi_u)^{-\frac{\nu_c}{2}}}\right)\mathrm{d}\phi\mathrm{d}r_i\right),\end{aligned} \tag{38}$$

where the conditional density is changed due to FFR as

$$\Lambda(r_i\mathrm{d}\phi\mathrm{d}r_i)=\frac{\lambda_d}{K_c}\frac{k(r_i)}{\mathcal{P}_r}r_i. \tag{39}$$

and ϕ_0 is given by

$$\phi_0=\begin{cases}\pi-\arccos\frac{r_i}{2R_{c_1}} & , \quad r_i<2R_{c_1}\\ \pi & , \quad \text{otherwise}\end{cases}, \tag{40}$$

where k_{r_i} is same with (32). With $\mathcal{L}_{I_{c_1}}(m)$ we could derive $\mathcal{C}_{c,e}$.

Since that, for the CEU, conditioned on C_0 not being retained, the coverage probability is

$$\begin{aligned}\mathcal{C}_{c,e}=\int_0^{R+R_m}&\frac{2\pi\lambda_c r_{c_1}\exp(-\pi\lambda_c r_{c_1}^2)}{1-\exp(-\pi\lambda_c(R+R_m)^2)}\\ &\cdot\exp\left(-\mathcal{N}_c r_{c_1}^{\nu_c}\right)\mathcal{L}_{I_{c_1}}\left(\gamma_c r_{c_1}^{\nu_c}\right)\mathrm{d}r_{c_1},\end{aligned} \tag{41}$$

where $\mathcal{N}_c=\frac{\gamma_c n_0}{P_c A_c}$ and $\mathcal{L}_{I_{c_1}}(m)$ is given by

$$\mathcal{L}_{I_{c_1}}\left(\gamma_c r_{c_1}^{\nu_c}\right)=\exp\left(-\int_{R_m}^{\infty}\int_{-\phi_0}^{\phi_0}\frac{\lambda_d}{K_c}\frac{k(r_i)}{\mathcal{P}_r}r_i \cdot\left(1-\frac{1}{1+\gamma_c r_{c_1}^{\nu_c}(r_{c_1}^2+r_i^2+2r_i r_{c_1}\cos\phi)^{\frac{-\nu_c}{2}}}\right)\mathrm{d}\phi\mathrm{d}r_i\right). \tag{42}$$

The overall coverage probability of C-plane is give by

$$\mathcal{C}_c=\mathcal{P}_r\mathcal{C}_{c,i}+(1-\mathcal{P}_r)\mathcal{C}_{c,e}. \tag{43}$$

VI. Delay Analysis

In this section, we will derive the delay performance of C/U-planes based on queueing theory and stochastic geometry. Since the proposed network is a multi-user system, traffic conditions play a major role in the queueing delay of the system. Therefore, we will first analyze the traffic of both planes.

The traffic of both C/U-planes is modeled by the $M/M/C$ queueing model [57], where C represents $C_{\{c,d\}}$, which denotes the available channels for C/U-planes. Specifically, we assume that a typical user's request arrives at its associated BS according to a Poisson process with a rate ω. Additionally, we assume that the user's requests are divided into two processes with probability p: one is the control requests with rate $\omega_c=p\omega$, and the other is the high-speed data requests with rate $\omega_d=(1-p)\omega$. Both processes follow independent Poisson processes, as described in [57].

Here, we assume that the ratio of reserved sub-bands for interior users is p_m. Consequently, the available channels for interior users and edge users are $p_m C_{\{c,d\}}$ and $(1-p_m)C_{\{c,d\}}/K_{\{c,d\}}$, respectively.

Due to the functional correlation between the CBSs and DBSs, we introduce a parameter α to describe the relationship between the total bandwidths of C/U-planes as $W_c = \alpha W_d$. This implies that operators should allocate a dedicated low-frequency band to assist the coverage of U-plane in high-frequency. Since the DBSs take advantage of the rich spectrum resources in high-frequency, α should be less than 1. Therefore, the bandwidths per channel for C/U-planes are $w_{\{c,d\}} = W_{\{c,d\}}/C_{\{c,d\}}$.

The average aggregated request arrival rate of a BS is $\Omega = \omega N$, where N represents the average number of users in the covered area of the BS. For DBSs, $N_d = S$ since users' distribution follows PCP, and N is equivalent to the cluster size. In contrast, for CBSs, $N_c = S/\mathcal{P}_r$. Consequently, the average aggregated request arrival rates for interior users and edge users of CBSs and DBSs are respectively given by

$$\Omega_{c,\{i,e\}} = \omega_c S \frac{\lambda_d}{\lambda_c} = \frac{p\omega S}{\mathcal{P}_r}\mathcal{P}_{c,\{i,e\}}, \tag{44}$$

and

$$\Omega_{d,\{i,e\}} = \omega_d S = (1-p)\omega S \mathcal{P}_{d,\{i,e\}}. \tag{45}$$

Then we will derive the delay performance of the network. According to [57], the probability that n requests are in the C-server queueing system (including the requests in queueing and in service), denoted by p_n, is

$$p_n = \begin{cases} p_0 \frac{(C\rho)^n}{n!}, & n \le C \\ p_0 \frac{\rho^n C^C}{C!}, & n > C \end{cases}, \tag{46}$$

where ρ and p_0 are given by

$$\rho = \frac{\Omega}{C\mu} < 1, \tag{47}$$

and

$$p_0 = \left[\sum_{n=0}^{C-1} \frac{(C\rho)^n}{n!} + \frac{(C\rho)^C}{C!(1-\rho)} \right]^{-1}, \tag{48}$$

where Ω is the request rate and μ is the service rate, i.e., the downlink transmitting rates of BSs.

The queueing probability that all servers are occupied, and new comers have to queue, is given according to *Erlang C formula* [57]:

$$\mathcal{P}_Q(\Omega, C, \mu) = \sum_{n=C}^{\infty} p_n = \frac{p_0 (C\rho)^C}{C!(1-\rho)}, \tag{49}$$

and the average queue length is given by

$$Q(\Omega, C, \mu) = \sum_{n=0}^{\infty} n p_{n+C} = \mathcal{P}_Q \frac{\rho}{1-\rho}. \tag{50}$$

Using *Little's Theorem* [57], the average delay T_Q that one request waiting in the queue is

$$T(\Omega, C, \mu) = \frac{Q}{\Omega}. \tag{51}$$

Inter-cell interferences lead to spatiotemporal interactions among the queues of different BSs, causing dependent queues of neighboring BSs and making the analysis more challenging. In [45-47], the authors made progress on the "interacting queue" problem under the mean-field approximation. However, in some more complex queueing models, this problem still remains to be addressed. When the service request arrival rates are stable, the queueing delay is determined by the downlink rates. Therefore, in this part, we attempt to analyze the queues based on the distributions of downlink rates.

Conditioned on the downlink rate of users competing for the same sub-band of one typical cell being X, the conditional expectation of queueing delay is given by

$$\mathbb{E}[T(\Omega, C, \mu)] = \mathbb{E}_X\{\mathbb{E}[T(\Omega, C, \mu) \mid \mu = X)]\}. \tag{52}$$

As a result, if we know the distribution of X, we could derive the expectation of delay T through the *Law of Total Expectation*:

$$\mathbb{E}[T(\Omega, C, \mu)] = \int_0^{\infty} \mathbb{E}[T(\Omega, C, \mu) \mid \mu = x] \mathrm{d}F_X(x). \tag{53}$$

where $F_X(x)$ is the CDF of rate X. For the distribution of rate X, we have derived the coverage probability of both C/U-planes in different conditions, which can be converted to the CDF of X, given by

$$\begin{aligned} F_X(x) &= \mathbb{P}(X < x) \\ &= \mathbb{P}(V \log_2(1+SINR) < x) \\ &= \mathbb{P}(SINR < 2^{\frac{x}{V}} - 1) \\ &= 1 - \mathcal{C}(\gamma(x) \mid \gamma(x) = 2^{\frac{x}{V}} - 1). \end{aligned} \tag{54}$$

where V denotes $V_{\{c,d\}} = w_{\{c,d\}}/B_{\{c,d\}}$, where $w_{\{c,d\}}$ is the bandwidth per channel for C/U-planes, respectively, and $B_{\{c,d\}}$ is the data size for one round transmission in C/U-planes, respectively.

The PDF of the rate, which is the derivative of $F_X(x)$, is

$$\begin{aligned} f_X(x) &= \frac{\mathrm{d}}{\mathrm{d}x} F_X(x) = \frac{\mathrm{d}}{\mathrm{d}\gamma(x)} F_X(\gamma(x)) \cdot \frac{\mathrm{d}}{\mathrm{d}x}\gamma(x) \\ &= -\frac{2^{\frac{x}{W}} \ln 2}{V} \{ \frac{\mathrm{d}}{\mathrm{d}\gamma(x)} \mathcal{C}(\gamma(x)) \mid \gamma(x) = 2^{\frac{x}{V}} - 1 \}. \end{aligned} \tag{55}$$

Therefore we need to derive the derivation of coverage probability $\mathcal{C}$ with respect to γ, which is list at the top of next page for different situation. Here, $\mathcal{G}_0 = {}_2F_1\left[1, 1-\frac{2}{\nu_d}, 2-\frac{2}{\nu_d}, -\gamma_d\right]$, $\mathcal{A}_0(r_i) = \lambda_d \frac{k(r_i)}{\mathcal{P}_r} r_i$, $\mathcal{B}_0(r_i, \phi_i) = r_{c_0}^{\nu_c}(r_{c_0}^2 + r_i^2 + 2r_i r_{c_0}\cos\phi)^{\frac{-\nu_c}{2}}$, $\mathcal{A}_1(r_i) = \frac{\lambda_d}{K_c}\frac{k(r_i)}{\mathcal{P}_r} r_i$ and $\mathcal{B}_1(r_i, \phi_i) = r_{c_1}^{\nu_c}(r_{c_1}^2 + r_i^2 + 2r_i r_{c_1}\cos\phi)^{\frac{-\nu_c}{2}}$.

Substituting $\mathrm{d}F_X(x) = f_X(x)\mathrm{d}x$ into (53), we could obtain the average queueing delay of C/U-planes' interior and edge users, denoted by $T_{c,i}$, $T_{c,e}$, $T_{d,i}$, and $T_{d,e}$, respectively.

The distribution of downlink rates X has taken the inter-cell interference into consideration. Although we cannot depict the coupling of interacting queues, we could still demonstrate the average delay performance of CUPS from the perspective of conditional expectation through the analysis above, and it will be verified through numerical results.

$$\frac{\mathrm{d}\mathcal{C}_{d,i}(\gamma_d)}{\mathrm{d}\gamma_d} = \frac{1}{\mathcal{P}_{d,i}} \int_0^R \exp\left(\mathcal{G}_d r_0^2 - \mathcal{N}_d r_0^{\nu_d}\right) \frac{2r_0}{R^2} \left(-2\lambda_d \pi r_0^2 \left(\frac{\frac{1}{1+\gamma_d} - \mathcal{G}_0}{\nu_d} + \frac{\mathcal{G}_0}{\nu_d - 2}\right) - \mathcal{N}_d \gamma_d\right) \mathrm{d}r_0. \tag{56}$$

$$\frac{\mathrm{d}\mathcal{C}_{d,e}(\gamma_d)}{\mathrm{d}\gamma_d} = \frac{1}{\mathcal{P}_{d,e}} \int_0^R \exp\left((\mathcal{G}'_d - \pi\lambda_d) r_1^2 - \mathcal{N}_d r_1^{\nu_d}\right) 2\pi\lambda_d r_1 \left(1 - \frac{r_1^2}{R^2}\right)$$
$$\cdot \left\{ \frac{2(\mathcal{L}_{I_0} - 1)}{\nu_d \gamma_d} \left(R^2 \mathcal{G}_1 - r_1^2 \mathcal{G}_2 + \frac{\gamma_d r_1^2}{\gamma_d + 1} - \frac{\gamma_d R^2}{\gamma_d + R^{\nu_d} r_1^{-\nu_d}}\right) + \left[-2\lambda_d \pi r_1^2 \left(\frac{\frac{1}{1+\gamma_d} - \mathcal{G}_0}{K_d \nu_d} + \frac{\mathcal{G}_0}{K_d(\nu_d - 2)}\right) - \mathcal{N}_d \gamma_d\right] \mathcal{L}_{I_0} \right\} \mathrm{d}r_1. \tag{57}$$

$$\frac{\mathrm{d}\mathcal{C}_{c,i}(\gamma_c)}{\mathrm{d}\gamma_c} = \int_0^R \exp\left(-\mathcal{N}_c r_{c0}^{\nu_c}\right) \mathcal{L}_{I_{c0}}\left(\gamma_c r_{c0}^{\nu_c}\right) \frac{2r_{c0}}{R^2} \left(-\mathcal{N}_c \gamma_c - \int_{R_m}^{\infty} \int_{-\pi}^{\pi} \frac{\mathcal{A}_0(r_i)\mathcal{B}_0(r_i, \phi_i)}{\left(1 + \gamma_c \mathcal{B}_0(r_i, \phi_i)\right)^2} \mathrm{d}\phi \mathrm{d}r_i\right) \mathrm{d}r_{c_0}. \tag{58}$$

$$\frac{\mathrm{d}\mathcal{C}_{c,e}(\gamma_c)}{\mathrm{d}\gamma_c} = \int_0^{R_m+R} f_{R_{c_1}}^{c,e}(r_{c_1}) \exp\left(-\mathcal{N}_c r_{c1}^{\nu_c}\right) \mathcal{L}_{I_{c_1}}\left(\gamma_c r_{c1}^{\nu_c}\right) \left(-\mathcal{N}_c \gamma_c - \int_{R_m}^{\infty} \int_{-\phi_0}^{\phi_0} \frac{\mathcal{A}_1(r_i)\mathcal{B}_1(r_i, \phi_i)}{\left(1 + \gamma_c \mathcal{B}_1(r_i, \phi_i)\right)^2} \mathrm{d}\phi \mathrm{d}r_i\right) \mathrm{d}r_{c_1}. \tag{59}$$

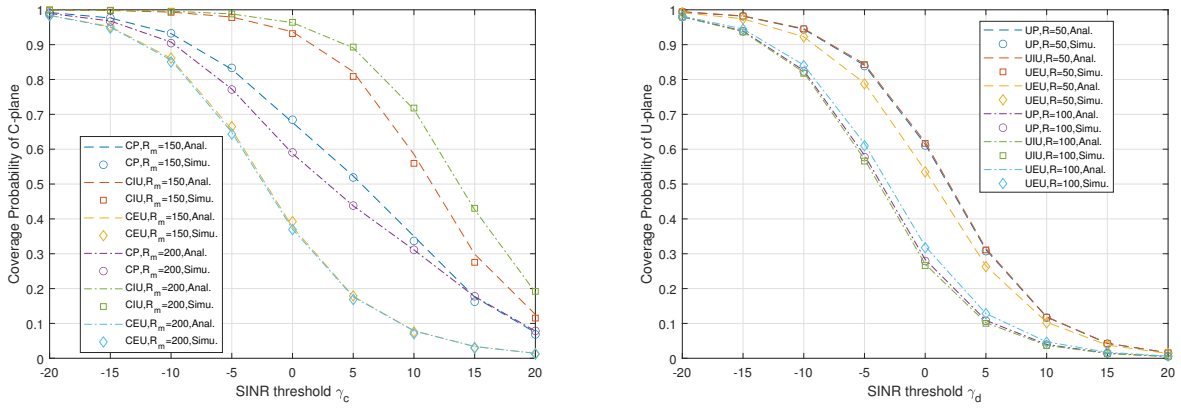

(a) Coverage probability of C-plane versus γ_c

(b) Coverage probability of U-plane versus γ_d

Fig. 3. Monte Carlo simulations of the overall, interior users' and edge users' coverage probability versus SINR threshold of (a) C-plane with different hard-core distance R_m and (b) U-plane with different cluster radius R.

VII. Numerical Results

To validate the performance advantage of the proposed schemes, numerical results are presented in this section. Throughout this section, the settings in Table I are used unless stated otherwise, where the parameters come from [11], [12].

TABLE I
PARAMETERS

	C-plane	U-plane
Channel number	$C_c = 50$	$C_d = 20$
Total bandwidth	$W_c = \alpha W_d, \alpha = 0.5$	$W_d = 20Mhz$
Transmit power	$P_c = 46dBm$	$P_d = 30dBm$
Threshold	$\gamma_c = -6dB$	$\gamma_d = -6dB$
Carrier frequency	$f_c = 2GHz$	$f_d = 6GHz$
FFR reuse factor	$K_c = 3$	$K_d = 3$
DBS density	$\lambda_d = 2 \times 10^{-5} BSs/m^2$	
Request rate	$\omega = 0.5$	
Separation factor	$p = 0.3$	
Noise power density	$n_c = n_d = -174dBm/Hz$	
Cluster size	$S = 10$	
Cluster radius	$R = 50m$	
Hard-core distance	$R_m = 100m$	

Adopting the path loss model from [12], the path losses for C/U-planes are respectively given by

$$\beta_c(dB) = 39 + 26\log_{10}(d[m]) + 20\log_{10}\left(\frac{f_c[GHz]}{5}\right), \tag{61}$$

$$\beta_d(dB) = 41 + 22.7\log_{10}(d[m]) + 20\log_{10}\left(\frac{f_d[GHz]}{5}\right), \tag{62}$$

which would determine the corresponding path gains A_c and A_d as well as the path loss exponents ν_c and ν_d of C/U-planes, and influence the SINR of C/U-planes in (3) and (4). By converting (61) and (62) to ratios, it could be obtained that $A_c = 7.87 \times 10^{-4}$, $\nu_c = 2.6$, $A_d = 5.52 \times 10^{-5}$, and $\nu_d = 2.27$.

Firstly, we verify the accuracy of the proposed analysis through Monte Carlo simulations in comparison with the theoretical derivations we derived in previous sections. In the case of FFR reuse factors $K_c = 1$ and $K_d = 1$, Fig. 3 shows the coverage probabilities of the interior users (marked by squares), the edge users (marked by diamonds),

This article has been accepted for publication in IEEE Transactions on Vehicular Technology. This is the author's version which has not been fully edited and content may change prior to final publication. Citation information: DOI 10.1109/TVT.2024.3350347

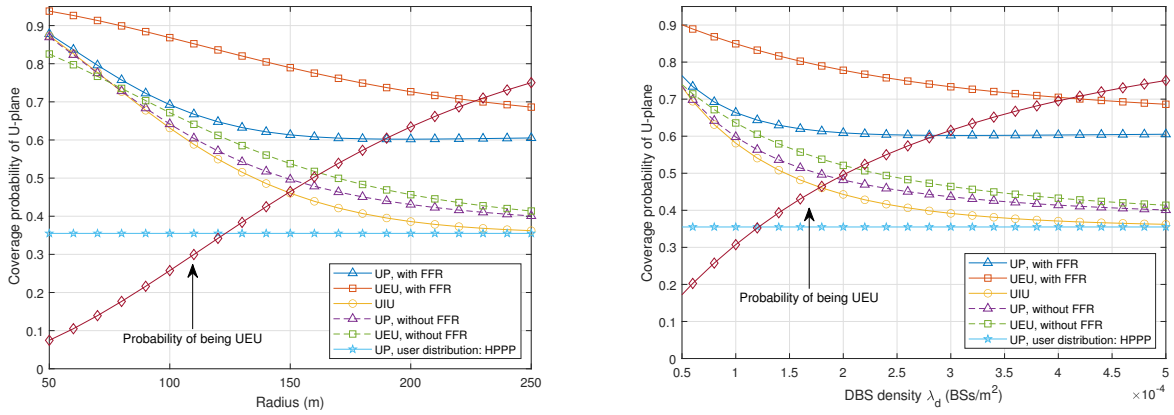

(a) Coverage probability of U-plane versus R

(b) Coverage probability of U-plane versus λ_d

Fig. 4. The overall, interior users' and edge users' coverage probability of U-plane versus (a) the radius of cluster and (b) the density of DBSs.

and the overall performance (marked by circles) of both C/U-planes versus SINR threshold. The analytical derivation of coverage probabilities of U-plane is perfectly matched with the simulation results. While for C-plane, the slight differences between the analytical and simulation results are caused by the approximation methods we adopted. We could also observe the variations of the U-plane coverage probability with different cluster radius R in Fig. 3(b), as well as the C-plane coverage probability with different hard-core distance R_m in Fig. 3(a), which are consistent with the results in Fig. 4 and Fig. 5.

Next, we demonstrate the coverage performance of U-plane users versus the range of the cluster and the density of DBSs in Fig. 4. The probability of the typical user being classified as UEU, i.e., $\mathcal{P}_{d,e}$ from (9), as well as the conditional coverage probabilities of U-plane users $\mathcal{C}_{d,i}$, $\mathcal{C}_{d,e}$, and $\mathcal{C}_d$ from (16), (22), and (23), are given in Fig. 4. We also make a comparison with the HPPP scheme in which users are independently distributed with DBSs following HPPP and not applying FFR, whose performance is independent of the cluster radius R. Since there are not center DBSs in the HPPP scheme, the proposed distance-based FFR cannot be applied. Hence, we also show coverage probabilities of the proposed scheme without applying FFR to make a fair comparison.

Fig. 4(a) shows that the coverage probabilities of both interior and edge users decrease with increasing R, because the contact distances for both UIUs and UEUs are less than R. A smaller cluster radius leads to higher SINR and better coverage probability. However, with the growth of the cluster range, the coverage probabilities of both UIUs and UEUs decrease because the associated DBS is further away. The probability of users being classified as UEUs is also illustrated in Fig. 4(a) and increases with the increase of R . The reason is that when the radius of the cluster is small, the overlapping between clusters is rare, leading to a lower probability of classifying the typical user as an edge user. Compared with the HPPP scheme, the coverage probability of the proposed PCP scheme is better, because the contact distance in the proposed PCP scheme is bounded by R. Additionally, if the distance-based FFR is not applied, the coverage probability of the proposed scheme will converge to that of the HPPP scheme. This is because, with the increase of R, the PCP will become increasingly similar to an ordinary PPP.

From Fig. 4(b) we can observe a similar conclusion to Fig. 4(a). As the DBS density increases, neighboring clusters have a higher probabilities to overlap with each other, and the overall user distribution will be similar to that of an ordinary PPP. Thus, D_0 is more difficult to be the nearest DBS. What should be noticed is that, in this observation, the cluster size is fixed, so the increase of DBS density cannot reduce the utilization of DBSs and lead to coverage enhancement. The coverage probability is reduced because the received signal power enhancement cannot offset the increased interference power.

From Fig. 4, we can obtain useful guidelines as follows. For a large cluster range or high DBS density, we can use PPP to approximate PCP and apply independent DBS deployment for CUPS; in other cases, the dependent BS deployment scheme is better. In other words, if the deployment of the DBSs is dense enough or the users are not concentrated enough, the necessity of dependent deployment will decline.

Fig. 5 demonstrates the coverage performance of the C-plane derived in (34), (41), and (43) with respect to the hard-core distance and the DBS density of the C-plane, respectively. In the proposed scheme, the CBS deployment is a dependent thinning of the DBS distribution based on MHCPs with retained probability P_r, where the minimum distance between any two CBSs is the hard-core distance R_m. To highlight the performance advantages of the proposed model, we introduced an independent thinning benchmark scheme (shown by dashed lines). In contrast, in the independent thinning scheme, the distribution of CBSs follows an independent HPPP, which is thinned from that of DBSs with the same probability P_r and is unrelated to the hard-core distance.

From Fig. 5 we can see that the proposed MHCP-based C-plane deployment outperforms the independent thinning scheme. When $R_m = 100\,\text{m}$ and $\lambda_d = 2 \times 10^{-5}\,\text{BS/m}^2$, compared to the independent thinning scheme, the proposed scheme demonstrates improvements in coverage probabilities of over 2, 11 and 4 percentage points for CIUs, CEUs, and C-plane overall, respectively. This superiority is attributed to

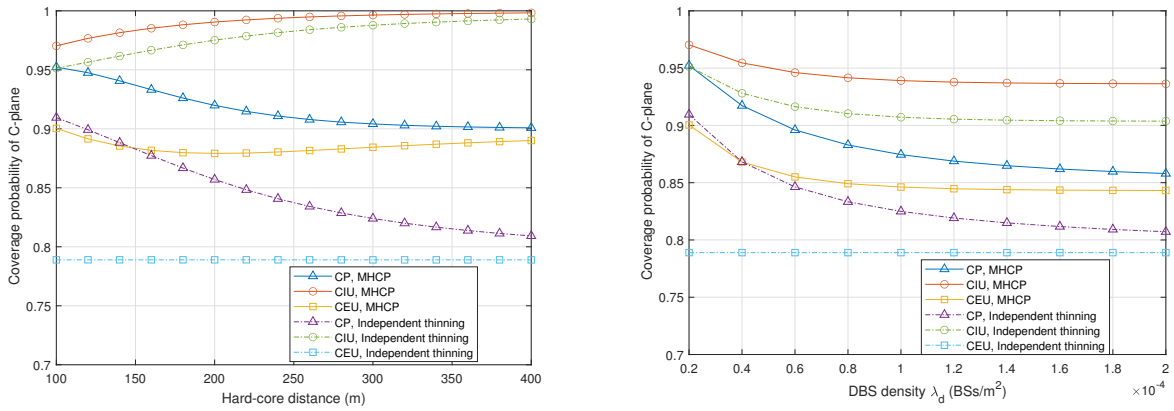

(a) Coverage probability of C-plane versus R_m

(b) Coverage probability of C-plane versus λ_d

Fig. 5. The overall, interior users' and edge users' coverage probability of C-plane users versus (a) the hare-core distance, and (b) the density of DBSs.

MHCPs ensuring sufficient distances to interfering CBSs. For CIUs, the coverage probability of the independent thinning scheme has similar trends but is worse than the proposed scheme based on MHCPs, because of the hard-core distance avoiding interfering CBSs to be arbitrarily close. However, for CEUs, there is a significant gap in coverage probability between the proposed and independent thinning schemes. Since the typical CEU is located in the cluster of an eliminated CBS with radius R, and the distance between the eliminated point and the nearest retained CBS is less than R_m, the contact distance of the typical CEU is less than $R + R_m$. This upper bound cannot be ensured in the independent thinning schemes, which is the reason for the gap.

As shown in Fig. 5(a), the coverage probabilities of CIUs increase from about 97% to 99% when R_m increasing to 200 m. Since we set a hard-core distance $R_m \geq 2R$, the clusters of CBSs do not overlap with each other, and CIUs will only associate with the center CBSs. Therefore, the increase in R_m does not affect their received signal power and makes interfering CBSs further and sparser, which results in the improvement of coverage probabilities. However, for the CEU, the coverage probability first decreases and then increases. This occurs because the increasing hard-core distance reduces both the received signal power and the interference power. The enlarged R_m not only decreases the density of interfering CBSs but also increases the contact distances of CEUs. The overall performance approaches that of CEUs since the proportion of CEUs is increasing.

In Fig. 5(b), we verify the coverage probability of the C-plane versus DBS density with a fixed hard-core distance. Note that here we analyze the performance of CBSs according to the density of DBSs rather than that of CBSs. The reason is that the CBS deployment is a dependent thinning of DBS deployment based on MHCP, and the relationship between the densities λ_c and λ_d is nonlinear. With the increasing λ_d, the density of CBSs λ_c first increases and then converges to a constant $\frac{1}{\pi R_m^2}$. In terms of the CIUs, the coverage decrease by about 3 percentage points when λ_d increasing to 1×10^{-4}BS/m^2. This is because, the interfering power grows with the increasing density of base stations, while the contact distance remains stable due to the fixed cluster radius. As for the CEUs, the contact distance is bounded by the unchanged $R + R_m$, so the coverage probabilities decrease with the increasing density of interfering CBSs.

The proposed scheme achieves an improvement in coverage probability of up to 10 percent after applying dependent thinning to deploy CBSs. Therefore, even with the same number of CBSs, the proposed deployment scheme with dependent thinning can significantly improve network coverage. This insight suggests that we should pay more attention to the deployment of base stations adapted to user distribution to achieve better network performance under limited resources.

The effectiveness of the proposed distance-based FFR scheme is demonstrated in Fig. 6. In the U-plane, as shown in Fig. 6(a), the proposed FFR scheme significantly enhances the coverage probability, especially in high inter-cell interference environments. Compared with the scenario where all edge users sharing the same channel ($K_d = 1$), the coverage probability increases from about 82% to 93% when K_d is increased to 3. This improvement is attributed to the efficient reduction of inter-cell interference at the edge users achieved by the proposed FFR scheme. Additionally, we compare with two cases in high inter-cell interference environments: (1) increasing the cluster radius R to 100 m and (2) increasing the DBS density λ_d to 2×10^{-4} BS/m^2. In both cases, for UEUs' or U-plane overall coverage probabilities, the proposed FFR scheme brings a more significant improvement. This is because increasing either R or λ_d leads to increased overlaps between clusters, leading to a larger proportion of edge users and greater inter-cell interference. Furthermore, due to the increased proportion of edge users, the impact of the improvement in coverage probability for edge users on the overall performance becomes more remarkable.

Fig. 6(b) demonstrates that the proposed distance-based FFR can effectively improve coverage probability in the C-plane. It can be observed that the coverage probability of edge users increases from about 74% to 90% as K_c grows from 1 to 3. The reason for this coverage improvement is that the reduction in inter-cell interference experienced by edge users with the increasing K_c. Similar to the U-plane, Fig.

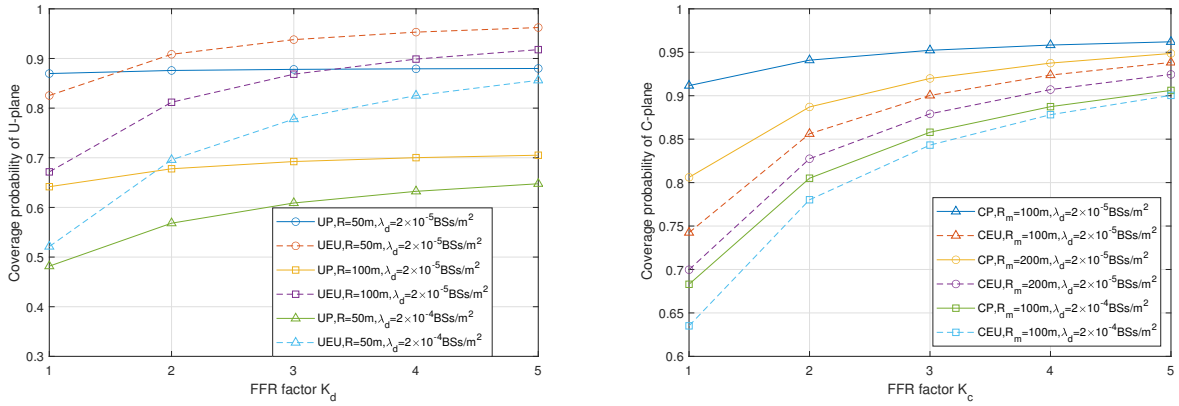

(a) Coverage probability of U-plane versus K_d

(b) Coverage probability of C-plane versus K_c

Fig. 6. The coverage probability of C/U-planes versus the FFR factors.

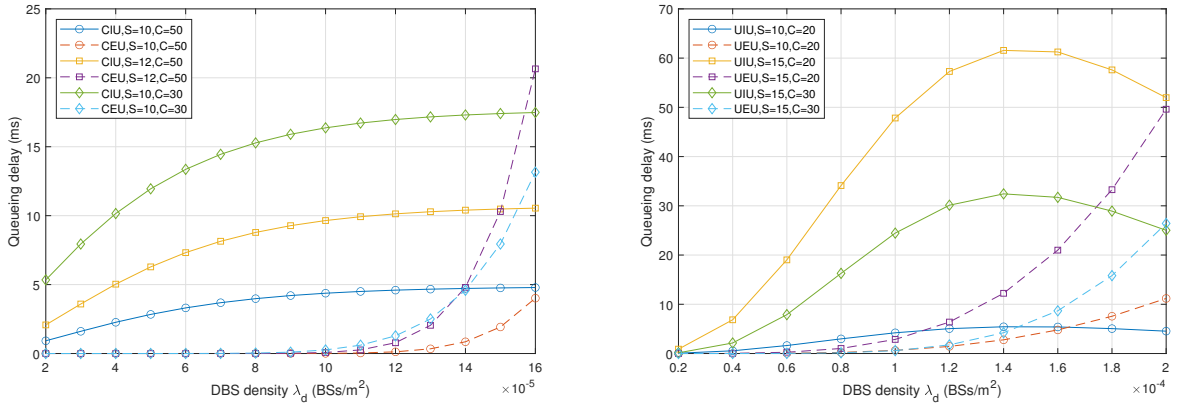

(a) Queueing delay of C-plane versus λ_d

(b) Queueing delay of U-plane versus λ_d

Fig. 7. The delay performance versus the density of DBSs of C/U-planes.

6(b) also shows that when inter-cell interference increases due to modifications in network deployment, such as changes in base station density and hard-core distance, the enhancement in coverage probabilities for both edge users and the overall C-plane becomes more significant.

Fig. 7 shows the queueing delay of both C/U-planes obtained in (53) in Section VI. The queueing latency is determined by the utilization rate $\rho = \frac{\Omega}{C\mu}$. When ρ approaches 1, there would be a sharp increase in the delay measure. Note that, $\rho < 1$ since otherwise the system cannot keep up with the request arrivals, and the delay will grow to infinity [57].

As there are dedicated sub-bands for interior and edge users according to FFR, each BS would have two independent queues for the associated interior and edge users. Therefore, we could separately analyze the queueing delay for interior and edge users. For CIUs, from (44) we can obtain that the $\Omega_{c,i} = \frac{p\omega S}{\mathcal{P}_r}\mathcal{P}_{c,i} = p\omega S$, which is irrelevant to λ_d, so that the queueing delay is inversely proportional to the rates. While for CEUs, the aggregated requests arrival rates $\Omega_{c,e}$ keep going up, resulting in the sharp increase of queueing delay, as shown in Fig. 7(a).

Since both $\Omega_{d,i}$ and the rates of UIU are declining with different variation tendencies, the queueing delay for UIU first increases and then decreases, as shown in Fig. 7(b). Finally, $\Omega_{d,i}$ will take the main role. In contrast, the rapid increase in the proportion of UEUs leads to the increasing queueing delay.

For both planes, the queueing delay of the interior users is limited compared to that of the edge users. The reasons can be divided into two aspects: (1) The proposed FFR strategies assign more users as edge users as the density of BSs increases. (2) Although FFR reduces the interference of edge users, it also reduces the available frequency band for edge users, which worsens the delay. Therefore, despite FFR improving the coverage probability of edge users, when designing FFR schemes, it is necessary to balance multiple performance aspects.

Fig. 8 shows the network performance versus the inter-tier interference under different performance metrics. Here we set a benchmark scheme in which C/U-planes are coupled, and both data and control signaling are transmitted by DBSs.

In the present model, DBSs operate in high-frequency bands to avoid limited spectrum resources in low-frequency bands and achieve high data rates. However, with the continuous development and utilization of high-frequency bands, the interference environment in these bands is becoming more complex. Here, we assume the existence of another micro-tier consisting of micro BSs operating in the frequency bands

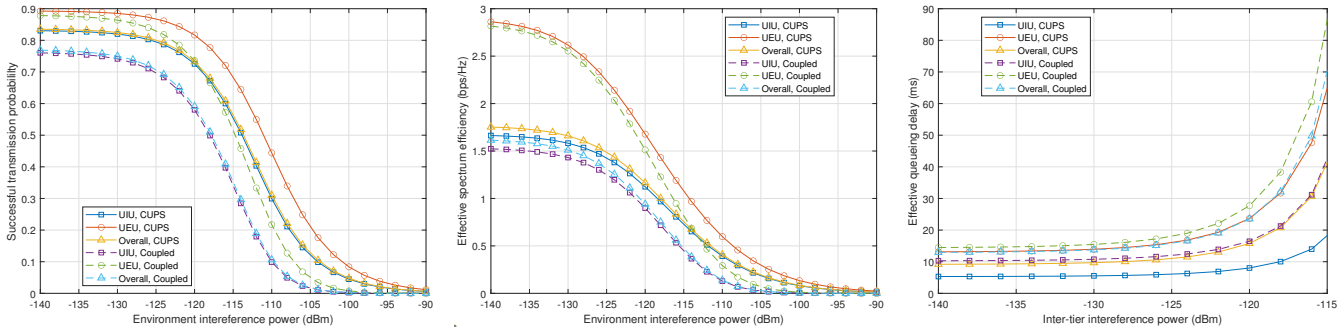

(a) Successful transmission probability (b) Effective spectral efficiency (c) Effective queueing delay

Fig. 8. The network performance versus inter-tier interference power under different performance metric: (a) Successful transmission probability. (b) Effective spectral efficiency. (c) Effective queueing delay.

of DBSs and deployed close to the proposed CUPS network [28], [54]. This micro-tier introduces additional inter-tier interference to users. Additionally, we assume there is no collaboration in terms of frequency sharing and reuse between the micro-tier and DBSs. To simplify the analysis, we omit the modeling and only consider the effect of inter-tier interference power in the high-frequency band, as shown in Fig. 8.

The CBS in the C-plane is responsible for transmitting essential control signaling, so the C-plane coverage of users should be considered in the U-plane and the overall coverage performance. We use $\mathcal{P}^{ST}$ to represent the successful transmission probability of a completed data transmission in the U-plane, as shown in Fig. 8(a). It is defined as $\mathcal{P}^{ST} = \mathcal{C}_c\mathcal{C}_d$, where $\mathcal{C}_c$ is from (43), and $\mathcal{C}_d$ is given by (16) and (22). Following a similar approach, effective spectrum efficiency (ESE) and effective queueing delay (EQD) are defined as the SE and queueing delay of a typical UP user under the coverage of a CBS: $\eta^{ESE} = \mathcal{C}_c\eta_d^{SE}$ and $T_d^E = T_d/\mathcal{C}_c$, where η_d^{SE} is derived from (25), and T_d is given by (53). These are shown in Fig. 8(b) and Fig. 8(c).

Since CBSs are operating in the stable and clean low-frequency band, in the presented model, CBSs can avoid the high-frequency inter-tier interference. From Fig. 8, it can be seen that the C/U coupled networks experience more performance loss from environmental interference, as both their control signaling and data are transmitted in the high-frequency band. In contrast, CUPS networks are more stable and are easier to maintain connectivity.

Fig. 8(c) compares the queueing delay of the proposed CUPS network with traditional coupled networks versus the inter-tier interference power with $\lambda_d = 2 \times 10^{-4}\,\text{BSs/m}^2$. The sharp increase is mainly caused by the decrease in transmission rates. It can be observed that the deterioration of queueing delay in the CUPS network is slower than that of the coupled network, which takes advantage of the stable channel environment of low-frequency CBSs.

VIII. Conclusion

In this paper, we investigate CUPS-based cellular networks in which control signaling and data are transmitted separately by CBSs and DBSs in the low and high-frequency bands, respectively. In particular, we consider the non-uniformly distributed users modeled by Poisson cluster processes (PCPs) and the correlated CBSs/DBSs deployment modeled by Matérn Hard Core Processes (MHCPs). Additionally, we propose two novel distance-based FFR techniques for C/U-planes, respectively, in which the classification of interior and edge users is based on the properties of MHCPs and PCPs. We derive expressions for coverage probability, spectrum efficiency, and queueing delay to analyze performance. Specifically, the queueing delay is examined based on an M/M/C queuing model according to the derived downlink rate distribution. Finally, in the numerical results, we verify the effectiveness of the proposed scheme by comparing it with the independent deployment scheme and the traditional C/U coupled network.

References

[1] G. Gui, M. Liu, F. Tang, N. Kato, and F. Adachi, "6G: Opening new horizons for integration of comfort, security, and intelligence," *IEEE Wirel. Commun.*, vol. 27, no. 5, pp. 126–132, 2020.

[2] G. Liu, X. Hou, Y. Huang, H. Shao, and Q. Wang, "Coverage enhancement and fundamental performance of 5G: Analysis and field trial," *IEEE Commun. Mag.*, vol. 57, no. 6, pp. 126–131, 2019.

[3] Z. Zhang, Y. Xiao, Z. Ma, M. Xiao, Z. Ding, X. Lei, G. K. Karagiannidis, and P. Fan, "6G wireless networks: Vision, requirements, architecture, and key technologies," *IEEE Veh. Technol. Mag.*, vol. 14, no. 3, pp. 28–41, 2019.

[4] S. Chen, Y. C. Liang, S. Sun, S. Kang, W. Cheng, and M. Peng, "Vision, requirements, and technology trend of 6G: How to tackle the challenges of system coverage, capacity, user data-rate and movement speed," *IEEE Wireless Commun.*, 2020.

[5] A. Papa, R. Durner, L. Goratti, T. Rasheed, and W. Kellerer, "Controlling next-generation software-defined RANs," *IEEE Commun. Mag.*, vol. 58, no. 7, pp. 58–64, 2020.

[6] K. Liang, L. Zhao, X. Chu, and H. Chen, "An integrated architecture for software defined and virtualized radio access networks with fog computing," *IEEE Netw.*, vol. 31, no. 1, pp. 80–87, 2017.

[7] A. Mohamed, O. Onireti, M. A. Imran, A. Imran, and R. Tafazolli, "Control-data separation architecture for cellular radio access networks: A survey and outlook," *IEEE Commun. Surveys Tuts.*, vol. 18, no. 1, pp. 446–465, 2017.

[8] Z. Chen, L. Qiu, and X. Liang, "Energy-efficient combination of small cells and multi-antenna under separation architecture," *IEEE Commun. Lett.*, vol. 19, no. 9, pp. 1572–1575, 2015.

[9] B. Yu, L. Yang, H. Ishii, and S. Mukherjee, "Dynamic TDD support in macrocell-assisted small cell architecture," *IEEE J. Sel. Areas Commun.*, vol. 33, no. 6, pp. 1201–1213, 2015.

[10] A. M. Abdelhady, O. Amin, and M. Alouini, "Energy-efficient resource allocation for phantom cellular networks with imperfect CSI," *IEEE Trans. Wireless Commun.*, vol. 16, no. 6, pp. 3799–3813, 2017.

[11] K. Liang, G. Liu, L. Zhao, X. Chu, S. Wang, and L. Hanzo, "Performance analysis of cellular radio access networks relying on control- and user-plane separation," *IEEE Trans. Veh. Technol.*, vol. 68, no. 7, pp. 7241–7245, 2019.

[12] H. Song, X. Fang, L. Yan, and Y. Fang, "Control/user plane decoupled architecture utilizing unlicensed bands in LTE systems," *IEEE Wirel. Commun.*, vol. 24, no. 5, pp. 132–142, 2017.

[13] H. Song, X. Fang, and C. Wang, "Cost-reliability tradeoff in licensed and unlicensed spectra interoperable networks with guaranteed user data rate requirements," *IEEE J. Sel. Areas Commun.*, vol. 35, no. 1, pp. 200–214, 2017.

[14] A. S. Mubarak, H. Esmaiel, and E. M. Mohamed, "LTE/Wi-Fi/mmWave RAN-level interworking using 2C/U plane splitting for future 5G networks," *IEEE Access*, vol. 6, pp. 53 473–53 488, 2018.

[15] S. Zhou, T. Zhao, Z. Niu, and S. Zhou, "Software-defined hyper-cellular architecture for green and elastic wireless access," *IEEE Commun. Mag.*, vol. 54, no. 1, pp. 12–19, 2016.

[16] Q. Li, W. Shi, X. Ge, and Z. Niu, "Cooperative edge caching in software-defined hyper-cellular networks," *IEEE J. Sel. Areas Commun.*, vol. 35, no. 11, pp. 2596–2605, 2017.

[17] D. Wu, J. Yan, H. Wang, and R. Wang, "User-centric edge sharing mechanism in software-defined ultra-dense networks," *IEEE J. Sel. Areas Commun.*, vol. 38, no. 7, pp. 1531–1541, 2020.

[18] Y. Hmamouche, M. Benjillali, S. Saoudi, H. Yanikomeroglu, and M. D. Renzo, "New trends in stochastic geometry for wireless networks: A tutorial and survey," *Proc. IEEE*, vol. 109, no. 7, pp. 1200–1252, 2021.

[19] S. Wang, L. Zhao, K. Liang, and G. Zheng, "Secrecy profits analysis of wireless-powered networks against randomly distributed eavesdroppers," in *2019 IEEE Int. Conf. Commun. (ICC)*, 2019, pp. 1–6.

[20] J. G. Andrews, F. Baccelli, and R. K. Ganti, "A tractable approach to coverage and rate in cellular networks," *IEEE Trans. Commun.*, vol. 59, no. 11, pp. 3122–3134, 2011.

[21] V. Suryaprakash, J. Møller, and G. Fettweis, "On the modeling and analysis of heterogeneous radio access networks using a poisson cluster process," *IEEE Trans. Wireless Commun.*, vol. 14, no. 2, pp. 1035–1047, 2015.

[22] S. M. Azimi-Abarghouyi, B. Makki, M. Haenggi, M. Nasiri-Kenari, and T. Svensson, "Stochastic geometry modeling and analysis of single- and multi-cluster wireless networks," *IEEE Trans. Commun.*, vol. 66, no. 10, pp. 4981–4996, 2018.

[23] M. Afshang, H. S. Dhillon, and P. H. J. Chong, "Fundamentals of cluster-centric content placement in cache-enabled device-to-device networks," *IEEE Trans. Commun.*, vol. 64, no. 6, pp. 2511–2526, 2016.

[24] W. Yi, Y. Liu, and A. Nallanathan, "Modeling and analysis of D2D millimeter-wave networks with poisson cluster processes," *IEEE Trans. Commun.*, vol. 65, no. 12, pp. 5574–5588, 2017.

[25] C. Saha, M. Afshang, and H. S. Dhillon, "3GPP-inspired hetnet model using poisson cluster process: Sum-product functionals and downlink coverage," *IEEE Trans. Commun.*, vol. 66, no. 5, pp. 2219–2234, 2018.

[26] P. D. Mankar, G. Das, and S. S. Pathak, "Modeling and coverage analysis of BS-centric clustered users in a random wireless network," *IEEE Wireless Commun. Lett.*, vol. 5, no. 2, pp. 208–211, 2016.

[27] M. Afshang and H. S. Dhillon, "Poisson cluster process based analysis of HetNets with correlated user and base station locations," *IEEE Trans. Wireless Commun.*, vol. 17, no. 4, pp. 2417–2431, 2018.

[28] C. Saha, M. Afshang, and H. S. Dhillon, "Enriched K -tier hetnet model to enable the analysis of user-centric small cell deployments," *IEEE Trans. Wireless Commun.*, vol. 16, no. 3, pp. 1593–1608, 2017.

[29] C. Saha, H. S. Dhillon, N. Miyoshi, and J. G. Andrews, "Unified analysis of HetNets using poisson cluster processes under max-power association," *IEEE Trans. Wireless Commun.*, vol. 18, no. 8, pp. 3797–3812, 2019.

[30] J. Lyu, H. M. Wang, and K. W. Huang, "Physical layer security in D2D underlay cellular networks with poisson cluster process," *IEEE Trans. Commun.*, vol. 68, no. 11, pp. 7123–7139, 2020.

[31] Y. Sun, Z. Ding, X. Dai, and O. A. Dobre, "On the performance of network NOMA in uplink CoMP systems: A stochastic geometry approach," *IEEE Trans. Commun.*, vol. 67, no. 7, pp. 5084–5098, 2019.

[32] H. Tabassum, E. Hossain, and J. Hossain, "Modeling and analysis of uplink non-orthogonal multiple access in large-scale cellular networks using poisson cluster processes," *IEEE Trans. Commun.*, vol. 65, no. 8, pp. 3555–3570, 2017.

[33] A. Ullah, Z. H. Abbas, F. Muhammad, G. Abbas, and S. Kim, "Uplink performance analysis of user- centric small cell aided dense HCNets with uplink-downlink decoupling," *IEEE Access*, vol. 8, pp. 148 460–148 474, 2020.

[34] M. Haenggi, "Mean interference in hard-core wireless networks," *IEEE Commun. Lett.*, vol. 15, no. 8, pp. 792–794, 2011.

[35] A. Al-Hourani and M. Haenggi, "Performance of next-generation cellular networks guarded with frequency reuse distance," *IEEE Trans. Commun.*, vol. 67, no. 10, pp. 7277–7287, 2019.

[36] A. Al-Hourani, R. J. Evans, and S. Kandeepan, "Nearest neighbor distance distribution in hard-core point processes," *IEEE Commun. Lett.*, vol. 20, no. 9, pp. 1872–1875, 2016.

[37] C. Chen, R. C. Elliott, and W. A. Krzymień, "Empirical distribution of nearest-transmitter distance in wireless networks modeled by matérn hard core point processes," *IEEE Trans. Veh. Technol.*, vol. 67, no. 2, pp. 1740–1749, 2018.

[38] Y. Chen and H. Zhang, "UAV networks through a spatial repulsion model," *IEEE Wireless Commun. Lett.*, vol. 11, no. 1, pp. 101–105, 2022.

[39] S. Zhang, Y. Zhu, and J. Liu, "Multi-UAV enabled aerial-ground integrated networks: A stochastic geometry analysis," *IEEE Trans. Wireless Commun.*, vol. 70, no. 10, pp. 7040–7054, 2022.

[40] H. He, J. Xue, T. Ratnarajah, F. A. Khan, and C. B. Papadias, "Modeling and analysis of cloud radio access networks using matérn hard-core point processes," *IEEE Trans. Wireless Commun.*, vol. 15, no. 6, pp. 4074–4087, 2016.

[41] Y. Zhong, T. Q. S. Quek, and X. Ge, "Heterogeneous cellular networks with spatio-temporal traffic: Delay analysis and scheduling," *IEEE J. Sel. Areas Commun.*, vol. 35, no. 6, pp. 1373–1386, 2017.

[42] M. Yang, H. Zhu, H. Qian, Y. Koucheryavy, K. Samouylov, and H. Wang, "Peer offloading with delayed feedback in fog networks," *IEEE Internet Things J.*, vol. 8, no. 17, pp. 13 690–13 702, 2021.

[43] B. Shi, F.-C. Zheng, C. She, J. Luo, and A. G. Burr, "Risk-resistant resource allocation for eMBB and URLLC coexistence under M/G/1 queueing model," *IEEE Trans. Veh. Technol.*, vol. 71, no. 6, pp. 6279–6290, 2022.

[44] H. H. Yang and T. Q. S. Quek, "Spatio-temporal analysis for SINR coverage in small cell networks," *IEEE Trans. Commun.*, vol. 67, no. 8, pp. 5520–5531, 2019.

[45] Y. Zhong, X. Ge, T. Han, Q. Li, and J. Zhang, "Tradeoff between delay and physical layer security in wireless networks," *IEEE J. Sel. Areas Commun.*, vol. 36, no. 7, pp. 1635–1647, 2018.

[46] H. H. Yang, T. Q. S. Quek, and H. Vincent Poor, "A unified framework for SINR analysis in poisson networks with traffic dynamics," *IEEE Trans. Commun.*, vol. 69, no. 1, pp. 326–339, 2021.

[47] X. Lu, M. Salehi, M. Haenggi, E. Hossain, and H. Jiang, "Stochastic geometry analysis of spatial-temporal performance in wireless networks: A tutorial," *IEEE Commun. Surveys Tuts.*, vol. 23, no. 4, pp. 2753–2801, 2021.

[48] J.-B. Seo and S.-Y. Kim, "Profit versus energy efficiency maximization in regular topology cellular networks," *IEEE Commun. Lett.*, vol. 20, no. 8, pp. 1643–1646, 2016.

[49] H. M. Al-Gunid, L. Zhao, J. Alshudukhi, Z. Wang, S. Li, and A. M. Sedimo, "Performance analysis of stratosphere cellular network relying on control- and user-plane separation," *IEEE Trans. Veh. Technol.*, vol. 71, no. 10, pp. 11 272–11 277, 2022.

[50] N. Saquib, E. Hossain, and D. I. Kim, "Fractional frequency reuse for interference management in lte-advanced hetnets," *IEEE Wireless Commun.*, vol. 20, no. 2, pp. 113–122, 2013.

[51] P. D. Mankar, G. Das, and S. S. Pathak, "Load-aware performance analysis of cell center/edge users in random hetnets," *IEEE Trans. Veh. Technol.*, vol. 67, no. 3, pp. 2476–2490, 2018.

[52] T. D. Novlan and J. G. Andrews, "Analytical evaluation of uplink fractional frequency reuse," *IEEE Trans. Commun.*, vol. 61, no. 5, pp. 2098–2108, 2013.

[53] A. D. Firouzabadi, A. M. Rabiei, and M. Vehkaperä, "Fractional frequency reuse in random hybrid fd/hd small cell networks with fractional power control," *IEEE Trans. Wireless Commun.*, vol. 20, no. 10, pp. 6691–6705, 2021.

[54] L. Yang, T. J. Lim, J. Zhao, and M. Motani, "Modeling and analysis of hetnets with interference management using poisson cluster process," *IEEE Trans. Veh. Technol.*, vol. 70, no. 11, pp. 12 039–12 054, 2021.

[55] E. Turgut and M. C. Gursoy, "Uplink performance analysis in D2D-enabled millimeter-wave cellular networks with clustered users," *IEEE Trans. Wireless Commun.*, vol. 18, no. 2, pp. 1085–1100, 2019.

[56] M. Haenggi and R. K. Ganti, *Interference in Large Wireless Networks*. Now Publishers Inc, 2009.

[57] D. P. Bertsekas and R. G. Gallager, *Data networks*. Prentice-Hall International New Jersey, 1992, vol. 3.

Shuai Wang received the B.Sc. degree in electronic information science and technology from Xidian University, Xi'an, China, in 2016, where he is currently working toward the Ph.D. degree with the School of Telecommunication Engineering. From 2019 to 2020, he was a Visiting Ph.D. Student with the School of Electronics and Computer Science, University of Southampton, Southampton, U.K., on the funds from the Program of the China Scholarship Council. His research interests include MIMO system, simultaneous wireless information and power transfer, and 6G wireless coverage enhancement.

Liqiang Zhao (Member, IEEE) received the B.Sc. degree in electrical engineering from Shanghai Jiao Tong University, China, in 1992, and the M.Sc. degree in communications and information systems and the Ph.D. degree in information and communications engineering from Xidian University, China, in 2000 and 2003, respectively.

From 1992 to 2005, he was a Research Engineer with the 20th Research Institute, Chinese Electronics Technology Group Corporation (CETC), China. From 2005 to 2007, he was an Associate Professor with the State Key Laboratory of Integrated Service Networks (ISN), Xidian University. He was appointed as a Marie Curie Research Fellow at the Centre for Wireless Network Design (CWiND), University of Bedfordshire, in June 2007, to conduct research in the GAWIND project funded under EU FP6 HRM Program. His activities focused on the area of automatic wireless broadband access network planning and optimization. Since June 2008, he has returned Xidian University, first as an Associate Professor and later as a Professor. He has hosted/participated many national research projects, such as the National Natural Science Foundation, the 863 Program, and the National Science Technology Major Projects, and several international research projects, including the EU FP6, FP7 plans for international cooperation exchange projects, and some research projects from companies, such as Huawei. He has more than 200 published in authorized academic periodicals both in and abroad and in international science conferences, wherein 60 of which are retrieved in SCI, and more than 140 of them are EI indexed, and more than 30 national invention patents. His current research interests include mobile communication systems, spread spectrum communications, broadband wireless communications, the space-air-ground integrated network, and the open-source network. In 2008, he was awarded by the Program for New Century Excellent Talents in University, Ministry of Education, China.

Kai Liang received the Ph.D. degree from the School of Telecommunications Engineering, Xidian University, China, in 2016. During 2014-2015, he visited the Network Convergence Laboratory, University of Essex, U.K., on the funds from the Program of the China Scholarships Council. He is currently an associate professor with the School of Telecommunications Engineering, Xidian University. He manages research projects funded by various sources such as NSFC, and the National Key R&D Program of China. His current research interests include network slicing, beamforming design for MIMO system, simultaneous wireless information and power transfer, and digital twins.

Gan Zheng (S'05-M'09-SM'12-F'21) received the BEng and the MEng from Tianjin University, Tianjin, China, in 2002 and 2004, respectively, both in Electronic and Information Engineering, and the PhD degree in Electrical and Electronic Engineering from The University of Hong Kong in 2008. He is currently Professor in Connected Systems in the School of Engineering, University of Warwick, UK. His research interests include machine learning for wireless communications, reconfigurable intelligent surface, UAV communications and edge computing. He is the first recipient for the 2013 IEEE Signal Processing Letters Best Paper Award, and he also received 2015 GLOBECOM Best Paper Award, and 2018 IEEE Technical Committee on Green Communications & Computing Best Paper Award. He was listed as a Highly Cited Researcher by Thomson Reuters/Clarivate Analytics in 2019. He currently serves as an Associate Editor for IEEE Wireless Communications Letters and IEEE Transactions on Communications.

Kai-Kit Wong (M'01-SM'08-F'16) received the BEng, the MPhil, and the PhD degrees, all in Electrical and Electronic Engineering, from the Hong Kong University of Science and Technology, Hong Kong, in 1996, 1998, and 2001, respectively. After graduation, he took up academic and research positions at the University of Hong Kong, Lucent Technologies, Bell-Labs, Holmdel, the Smart Antennas Research Group of Stanford University, and the University of Hull, UK. He is Chair in Wireless Communications at the Department of Electronic and Electrical Engineering, University College London, UK. His current research centers around 6G and beyond mobile communications. He is Fellow of IEEE and IET. He served as the Editor-in-Chief for IEEE Wireless Communications Letters between 2020 and 2023.